

PHOTOELECTROCHEMICAL OXIDATION OF BENZYL ALCOHOL IN A CONTINUOUS-FLOW  
MICROCHANNEL REACTOR USING TITANIUM DIOXIDE PHOTOANODE



A Thesis Submitted in Partial Fulfillment of the Requirements  
for the Degree of Master of Engineering in Chemical Engineering  
Department of Chemical Engineering  
Faculty Of Engineering  
Chulalongkorn University  
Academic Year 2023

ปฏิกริยาโฟโตอิเล็กโตรเคมีคอลออกซิเดชันของเบนซิลแอลกอฮอล์ในเครื่องปฏิกริยาไมโครเซนแนล  
แบบต่อเนื่องโดยใช้โฟโตแอโนดไทเทเนียมไดออกไซด์



วิทยานิพนธ์นี้เป็นส่วนหนึ่งของการศึกษาตามหลักสูตรปริญญาวิศวกรรมศาสตรมหาบัณฑิต  
สาขาวิชาวิศวกรรมเคมี ภาควิชาวิศวกรรมเคมี  
คณะวิศวกรรมศาสตร์ จุฬาลงกรณ์มหาวิทยาลัย  
ปีการศึกษา 2566

Thesis Title PHOTOELECTROCHEMICAL OXIDATION OF BENZYL ALCOHOL IN  
A CONTINUOUS-FLOW MICROCHANNEL REACTOR USING  
TITANIUM DIOXIDE PHOTOANODE

By Mr. Sirachat Sattayarak

Field of Study Chemical Engineering

Thesis Advisor Associate Professor Paravee Vas-Umnuay

---

Accepted by the FACULTY OF ENGINEERING, Chulalongkorn University in Partial  
Fulfillment of the Requirement for the Master of Engineering

..... Dean of the FACULTY OF ENGINEERING  
(Professor SUPOT TEACHAVORASINSKUN)

THESIS COMMITTEE

..... Chairman  
(Professor MUENDUEN PHISALAPHONG)

..... Thesis Advisor  
(Associate Professor Paravee Vas-Umnuay)

..... Examiner  
(Assistant Professor CHALIDA KLAYSOM)

..... External Examiner  
(Tanyakorn Muangnapoh)

จุฬาลงกรณ์มหาวิทยาลัย  
CHULALONGKORN UNIVERSITY

ศิริชัช สัตยารักษ์ : ปฏิกริยาโฟโตอิเล็กโทรเคมีคอลออกซิเดชันของเบนซิลแอลกอฮอล์ในเครื่อง  
 ปฏิกริยาไมโครแชนแนลแบบต่อเนื่องโดยใช้โฟโตแอโนดไทเทเนียมไดออกไซด์. (   
 PHOTOELECTROCHEMICAL OXIDATION OF BENZYL ALCOHOL IN A CONTINUOUS-  
 FLOW MICROCHANNEL REACTOR USING TITANIUM DIOXIDE PHOTOANODE) อ.ที่ปรึกษา  
 หลัก : รศ. ดร.ปารวี วาศน์อำนวนย

เชื้อเพลิงฟอสซิลซึ่งเป็นแหล่งพลังงานหลักของมนุษย์จะปลดปล่อยแก๊สคาร์บอนไดออกไซด์และแก๊ส  
 เรือนกระจกส่งผลเสียต่อสิ่งแวดล้อม เพื่อแก้ปัญหาดังกล่าวการพัฒนาเทคโนโลยีเพื่อผลิตพลังงานหมุนเวียนจึง  
 เป็นสิ่งสำคัญ แสงอาทิตย์เป็นแหล่งพลังงานหมุนเวียนที่มีอยู่อย่างไม่จำกัดและกำลังได้รับความสนใจเพื่อนำมา  
 ประยุกต์ใช้เพื่อให้เกิดประโยชน์ทั้งในด้านการผลิตพลังงานและการเร่งปฏิกริยาเคมี เซลล์ไฟฟ้าเคมีทางแสงเป็น  
 เทคนิคที่ใช้เพื่อเร่งปฏิกริยา โดยเป็นการผสมผสานระหว่างเซลล์ไฟฟ้าเคมีและการเร่งปฏิกริยาด้วยแสง ข้อดีของ  
 ระบบนี้คือการใช้พลังงานต่ำเพื่อเร่งปฏิกริยาจากการกระตุ้นด้วยพลังงานแสงอาทิตย์ ในงานวิจัยนี้เครื่องปฏิกริยา  
 เซลล์ไฟฟ้าเคมีทางแสงแบบต่อเนื่องถูกพัฒนาขึ้นเพื่อออกซิเดชันเบนซิลแอลกอฮอล์ไปเป็นเบนซาลดีไฮด์ โดยจะ  
 ศึกษาผลกระทบที่อัตราการไหลของสารละลายอิเล็กโทรไลต์ระหว่าง 0.05 ถึง 0.20 มิลลิลิตรต่อนาที ส่งผลต่อค่า  
 การเปลี่ยนแปลงเบนซิลแอลกอฮอล์และค่าการเลือกเกิดเบนซาลดีไฮด์ ส่วนประกอบที่สำคัญในเซลล์ไฟฟ้าเคมี  
 ทางแสงคือโฟโตอิเล็กโทรดสำหรับใช้ในการเร่งปฏิกริยา งานวิจัยนี้จะศึกษาฟิล์มไทเทเนียมไดออกไซด์ที่มีลักษณะ  
 แตกต่างกัน 2 แบบได้แก่ ฟิล์มแบบแข็งและฟิล์มแบบมีรูพรุน ซึ่งถูกใช้เป็นขั้วโฟโตแอโนดสำหรับปฏิกริยาไฟฟ้า  
 เคมีทางแสง จากผลการทดลองพบว่าอัตราการไหลที่เพิ่มขึ้นส่งผลให้ค่าอัตราการเปลี่ยนแปลงของเบนซิล  
 แอลกอฮอล์มีค่าลดลง ในขณะที่ค่าเลือกเกิดเบนซาลดีไฮด์จะมีค่าเพิ่มขึ้น ในสภาวะที่ดีที่สุดพบว่าการใช้ฟิล์มแบบ  
 แข็งสามารถให้ค่าการเลือกเกิดเบนซาลดีไฮด์สูงสุดที่ 43.11% ที่อัตราการไหล 0.1 มิลลิลิตรต่อนาที และมีค่าการ  
 เปลี่ยนแปลงเบนซิลแอลกอฮอล์อยู่ที่ 55.98% สำหรับฟิล์มแบบมีรูพรุนมีค่าการเลือกเกิดเบนซาลดีไฮด์อยู่ที่  
 50.59% และมีค่าการเปลี่ยนแปลงเบนซิลแอลกอฮอล์ 42.20% ที่อัตราการไหล 0.15 มิลลิลิตรต่อนาที

สาขาวิชา วิศวกรรมเคมี  
 ปีการศึกษา 2566

ลายมือชื่อนิสิต .....  
 ลายมือชื่อ อ.ที่ปรึกษาหลัก .....

# # 6472080621 : MAJOR CHEMICAL ENGINEERING

KEYWORD: Photoelectrochemical, Continuous flow system, Titanium dioxide,  
Benzaldehyde

Sirachat Sattayarak : PHOTOELECTROCHEMICAL OXIDATION OF BENZYL ALCOHOL IN A  
CONTINUOUS-FLOW MICROCHANNEL REACTOR USING TITANIUM DIOXIDE  
PHOTOANODE. Advisor: Assoc. Prof. Paravee Vas-Umnuay

Fossil fuel, a primary energy source of humans, emits carbon dioxide and other greenhouse gases which have a high impact on the environment. Renewable energy development has been promised to solve the problem. Solar light, a renewable energy with an unlimited energy source, has gained attention to develop in various applications including energy production and catalytic chemical reactions. The photoelectrochemical process is a chemical catalysis technique that combines electrochemical and photocatalysis and has an advantage of low energy consumption due to solar energy support. In this work, the continuous-flow photoelectrochemical reactor was fabricated to undergo the oxidation reaction of benzyl alcohol into benzaldehyde. This work investigated the effects of electrolyte flow rate ranging from 0.05 to 0.20 ml/min on the percentage conversion of benzyl alcohol and the percentage selectivity of benzaldehyde. The most important part of a photoelectrochemical cell is photoelectrode for catalysis of the chemical reaction. Two different morphologies of  $\text{TiO}_2$ , which are compact and mesoporous films were used as photoanodes for the photoelectrochemical reaction. The results showed that when the electrolyte flow rate was increased, the conversion was decreased, while the selectivity was increased. At the optimal conditions, the benzaldehyde selectivity of 43.11% was obtained when using the compact  $\text{TiO}_2$  film with the electrolyte flow rate of 0.1 ml/min (where the conversion is 55.98%). While for the mesoporous  $\text{TiO}_2$  film, 50.59% selectivity of benzaldehyde and 42.20% conversion was obtained at the electrolyte flow rate of 0.15 ml/min.

Field of Study: Chemical Engineering

Student's Signature .....

Academic Year: 2023

Advisor's Signature .....

## ACKNOWLEDGEMENTS

First, I would like to express my deepest and sincere gratitude to my advisor, Associate Professor Paravee Vas-Umnuay, Ph.D., Department of Chemical Engineering, Chulalongkorn University. For providing opportunities, suggestion and supporting throughout of my study in chemical engineering.

I would like to gratitude to Professor Muenduen Phisalaphong, Assistant Professor Chalida Klaysom, Dr. Tanyakorn Muangnapoh, members of thesis committee for their participation and giving helpful suggestion and comment.

This work was supported by Center of Excellence in Particle and Material Processing Technology (CEPT) under Department of Chemical Engineering, Faculty of Engineering, Chulalongkorn University

Finally, my thesis could not be accomplished without my parents for giving me an opportunity, encouragement and support me until graduated. I also would like to thanks members of the Center of Excellence in Particle Technology for useful advice, support and cooperation.

Sirachat Sattayarak

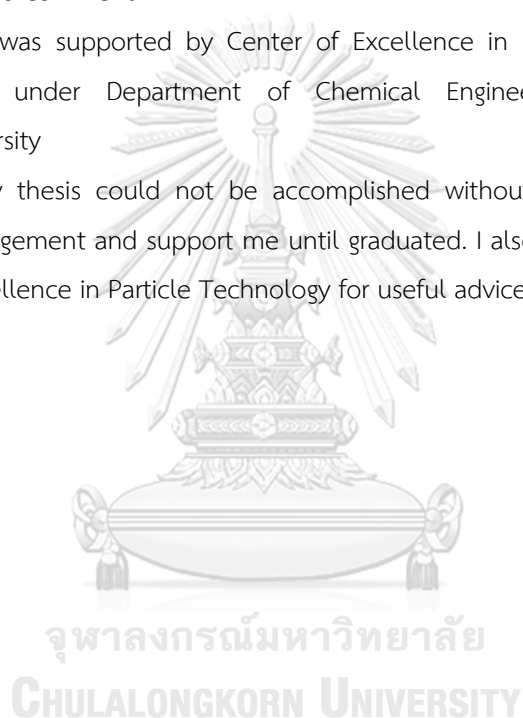


## TABLE OF CONTENTS

	Page
ABSTRACT (THAI).....	iii
ABSTRACT (ENGLISH).....	iv
ACKNOWLEDGEMENTS.....	v
TABLE OF CONTENTS.....	vi
LIST OF TABLES.....	ix
Table of figures.....	x
CHAPTER 1.....	1
1.1 Background.....	1
1.2 Objectives.....	2
1.3 Scopes of research.....	3
1.4 Expected Benefits.....	3
CHAPTER 2.....	4
2.1 Benzyl alcohol.....	4
2.2 Benzaldehyde.....	4
2.2.1 Conventional method.....	5
2.2.2 Oxidation of benzyl alcohol.....	5
2.3 Hydrogen production.....	6
2.3.1 Steam reforming.....	6
2.3.2 Partial oxidation.....	7
2.3.3 Coal gasification.....	7
2.3.4 Hydrogen production from biomass.....	8

2.3.5 Water splitting.....	8
2.4 Photoelectrochemical cell.....	9
2.4.1 Photoelectrochemical cell water splitting .....	10
2.4.2 Photoelectrochemical cell for benzyl alcohol oxidation.....	11
2.5 Titanium dioxide.....	13
2.5.1 Synthesis of TiO <sub>2</sub> nanoparticles .....	14
2.5.2 Thin film deposition of TiO <sub>2</sub> .....	17
2.6 Literature review.....	22
2.6.1 Photo-electrocatalytic .....	23
2.6.2 Electrocatalytic.....	23
2.6.3 Photocatalytic.....	24
2.6.4 Catalytic .....	25
2.6.5 Simulation of photoelectrochemical cell.....	26
2.6.6 Literature review summary .....	28
CHAPTER 3.....	30
3.1 Chemicals and Equipment .....	30
3.1.1 Chemicals .....	30
3.1.2 Equipment.....	30
3.2 Experimental.....	31
3.2.1 Synthesis of TiO <sub>2</sub> thin film photoanode .....	31
3.2.2 Membrane activation .....	32
3.2.3 Oxidation of benzyl alcohol via photoelectrochemical reactor.....	32
3.3 Characterization.....	34
CHAPTER 4.....	35



4.1 Morphology and structure of compact and mesoporous TiO <sub>2</sub> films.....	35
4.1.1 Morphology characterization.....	35
4.1.2 Structure characterization.....	36
4.1.3 Surface area analysis.....	37
4.2 Optical and electrical properties of compact and mesoporous TiO <sub>2</sub> films.....	39
4.2.1 Optical properties.....	39
4.2.2 Electrical properties.....	40
4.3 Photoelectrochemical oxidation of benzyl alcohol.....	41
4.3.1 Standard calibration.....	41
4.3.2 Effect of electrolyte flow rate on benzyl alcohol conversion.....	42
4.3.3 Effect of electrolyte flow rate on benzaldehyde selectivity.....	44
4.3.4 The proposed reaction pathways of benzyl alcohol.....	45
4.3.5 Effect of other factors on percentage conversion and selectivity.....	46
CHAPTER 5.....	50
5.1 Conclusion.....	50
5.2 Recommendation.....	50
REFERENCES.....	53
VITA.....	59

## LIST OF TABLES

	Page
Table 1 Physical properties and structure of TiO <sub>2</sub> .....	14
Table 2 Literature review summary .....	22
Table 3 Specific surface area of mesoporous TiO <sub>2</sub> film .....	39
Table 4 The relationship between concentration and area of chromatogram .....	42
Table 5 Benzaldehyde percentage selectivity using mesoporous and compact film after 1.5 hr.....	45
Table 6 Performance comparison of PEC oxidation of benzyl alcohol under different conditions.....	48
Table 7 Performance comparison of PEC oxidation of benzyl alcohol to recent literature.....	48

## Table of figures

	Page
Figure 2.1 Hydrolysis of benzyl chloride to benzyl alcohol.....	4
Figure 2.2 Hydrolysis of benzal chloride to benzaldehyde.....	5
Figure 2.3 Air oxidation of toluene to benzaldehyde.....	5
Figure 2.4 Oxidation of benzyl alcohol.....	6
Figure 2.5 Percentage of hydrogen production source [18] .....	6
Figure 2.6 Natural gas steam reforming process [19].....	7
Figure 2.7 Coal gasification process. [19].....	8
Figure 2.8 (a) Photoelectrochemical cell component. (b) n-type semiconductor photoelectrochemical cell. (c) n-type semiconductor photoelectrochemical cell. (d) Dual photoelectrochemical cell.....	10
Figure 2.9 Schematic diagram of photoelectrochemical cell of water splitting. ....	11
Figure 2.10 Schematic diagram of photoelectrochemical oxidation of benzyl alcohol. ....	12
Figure 2.11 (a) Band diagram of photoelectrochemical cell of water splitting. (b) Band diagram of photoelectrochemical cell of benzyl alcohol oxidation to benzaldehyde.....	13
Figure 2.12 Schematic diagram of sol-gel method.....	15
Figure 2.13 Mechanism of TiO <sub>2</sub> synthesized via sol-gel method using TTIP. ....	15
Figure 2.14 Schematic diagram of hydrothermal and solvothermal method. ....	16
Figure 2.15 Classification of thin film deposition technique. ....	17
Figure 2.16 Schematic diagram of chemical vapor deposition. ....	18
Figure 2.17 Schematic diagram of physical vapor deposition.....	19

Figure 2.18 Procedure of spin-coating methods.....	20
Figure 2.19 Procedure of dip-coating method. ....	20
Figure 2.20 Schematic diagram of doctor blade.....	21
Figure 2.21 Schematic diagram of a convective deposition.....	21
Figure 2.22 Proposed mechanism of benzyl alcohol oxidation via linear paired electrolysis. [41].....	24
Figure 2.23 Schematic diagram of membrane microchannel reactor. A: Pump, B: Preheater, C: Gas pressure gauge, D: mass flow controller, E: backpressure valve, F: Gas-liquid separator, G: Condenser [46].....	26
Figure 2.24 Photoelectrochemical chamber flow distribution. [47] .....	27
Figure 2.25 Hydrogen and oxygen concentration profile in photoelectrochemical cell [48].....	27
Figure 2.26 Flat plate continuous flow photoelectrochemical reactor consist of a) Anode, b) Nafion membrane, c) Platinized-Titanium cathode, d) Quartz window, e) Body plate, f) nitrile gaskets. [49].....	28
Figure 2.27 Effect of electrolyte flow rate on development of O <sub>2</sub> saturation in the electrolyte a) 6×10 <sup>-5</sup> m <sup>3</sup> /min, b) 15×10 <sup>-5</sup> m <sup>3</sup> /min. [49].....	28
Figure 3.1 Photoelectrochemical reactor component.....	32
Figure 3.2 Schematic diagram of the photoelectrochemical system.....	33
Figure 4.1 SEM micrographs showing (a) surface morphology of mesoporous TiO <sub>2</sub> film (b) cross-sectional image of mesoporous TiO <sub>2</sub> film, (c) surface morphology of compact TiO <sub>2</sub> film, and (d) cross-sectional image of compact TiO <sub>2</sub> film.....	36
Figure 4.2 XRD patterns of compact (black) and mesoporous (red) TiO <sub>2</sub> films deposited on FTO glasses.....	37
Figure 4.3 N <sub>2</sub> adsorption and desorption isotherm of mesoporous TiO <sub>2</sub> film.....	38
Figure 4.4 Pore size distribution of mesoporous TiO <sub>2</sub> film.....	39

Figure 4.5 Optical analysis of (a, c) UV-Vis absorbance, and (b, d) optical band gap energy of compact and mesoporous TiO <sub>2</sub> films. ....	40
Figure 4.6 Cyclic voltammetry of (a) Mesoporous TiO <sub>2</sub> film and (b) Compact TiO <sub>2</sub> film. ....	41
Figure 4.7 HPLC Chromatograms of the standard of (a) benzyl alcohol and (b) benzaldehyde.....	42
Figure 4.8 Effect of electrolyte flow rate on conversion of benzyl alcohol.....	43
Figure 4.9 Comparison of conversion of benzyl alcohol using mesoporous and compact TiO <sub>2</sub> films as photoanode at flow rates of (a) 0.05, 0.1 ml/min and (b) 0.15, 0.2 ml/min.....	44
Figure 4.10 The reaction pathways of benzyl alcohol. ....	46
Figure 4.11 Photoelectrochemical effects from different factors on (a) benzyl alcohol conversion and (b) benzaldehyde selectivity.....	47

# CHAPTER 1

## INTRODUCTION

### 1.1 Background

In the past 1-2 centuries since the industrial revolution, industrial technologies have been developed to achieve the demand of humans. The growth of the technologies is followed by the impact on the environment, such as the burnout of fossil fuels, air pollution, and wastewater emission. [1] To replace the limited fossil energy, sustainable technologies, and alternative energies, which are the key to solving this problem, are gaining attention and being developed to replace fossil fuels. Solar energy is an unlimited energy source that is applied to various applications including energy production or catalysis chemical reactions in wastewater treatment, conversion of CO<sub>2</sub>, degradation of biomass, and essentially conversion of biomass into a valuable product.

Photoelectrochemical (PEC) process is a technique that applies solar light and electricity for catalytic chemical reactions. The simplest system of PEC cells is water splitting, invented by Honda and Fujishima in 1972, which aims for hydrogen production and oxygen as a byproduct. [2] The system contains a semiconductor material used as a photoanode and a metal used as a cathode. When the semiconductor is excited by the light in which the energy is beyond the band gap of the semiconductor, electrons at the valence band will be excited, then transfer into the conduction band, generating photogenerated electron (e<sup>-</sup>) and leaving hole (h<sup>+</sup>) at the valence band. Water then reacts with holes to form oxygen and protons, called the oxygen evolution reaction. This reaction has a reduction potential of 1.23 V., Electrons on the other hand will transfer through an external wire and combine with proton on the cathode side to form hydrogen, which is called hydrogen evolution reaction. [3] The disadvantages of water splitting reaction are the large amount of electricity required and the slow oxygen evolution reaction, resulting in the rate-limiting step of the overall reaction. [4] Therefore, it is suitable to substitute oxygen evolution reaction with photo-oxidation of biomass. Since most biomass sources have a reduction potential of about -0.02 to 0.26 V, which means less energy is utilized and the product will be replaced with a more valuable product. [5] Moreover, raw biomass materials are available in many industries including agriculture, food and beverage, and biofuel production. [6] Benzaldehyde, the simplest form of aromatic aldehyde, is often used as a precursor in the production of complex aldehydes in the pharmaceutical industry and the dye industry. In general, there are two industrial production methods of benzaldehyde: (i) Chlorination and

hydrolysis of toluene, which requires high temperature and high pressure, and (ii) Air oxidation of toluene. The major drawback is the reaction requires an expensive catalyst or a complex system. Therefore, PEC process can be a promising alternative. The most important part of the PEC system is an electrode. The best candidate for anode side is  $\text{TiO}_2$  which is a semiconductor that is widely studied in the photocatalysis field due to its non-toxicity, cheapness, and essentially high physical and chemical stability. However, a large band gap of 3.2 eV for the anatase phase of  $\text{TiO}_2$  limits the absorption wavelength to only in the UV region. Therefore, there are several ways to improve  $\text{TiO}_2$  efficiency including doping with cations or anions, combining with visible light active photocatalyst, and even modify the nanostructure which is also an important role in the PEC study [4, 7]. Many researchers studied the oxidation of benzyl alcohol to benzaldehyde via PEC process. Z. Zhou et al. used  $\text{Bi}_2\text{MoO}_6/\text{TiO}_2$  as a photoanode and  $\text{C}/\text{Cu}_2\text{O}$  as a photocathode, resulting in 67.4% benzyl alcohol conversion and 98.6% benzaldehyde selectivity. [4]. Also, Z. Wu et al. used  $\text{Au}/\text{TiO}_2$  nanotube as a photoanode and  $\text{C}/\text{Cu}_2\text{O}$  NW as a photocathode to achieve 84.68% benzyl alcohol conversion and more than 99% benzaldehyde selectivity. [5] However, so far these have been studies focusing only on a batch system. No studies in a continuous system have been reported yet.

In this work, a continuous flow PEC reactor has been designed for the oxidation of benzyl alcohol to benzaldehyde with sodium sulfate solution as an electrolyte. The reactor consists of two types of morphologies of  $\text{TiO}_2$  photoanode, compact film and mesoporous film, which were synthesized via a sol-gel method. These two different morphologies are expected to have different surface areas, which could result in different conversion and selectivity of the product. Because a large-scale substrate was used for photoanode film deposition, the convective deposition technique was chosen for film deposition due to the low precursor needed and required uncomplicated system compared to other methods. The other main component of the PEC reactor is a copper plate used as a cathode, Nafion 117 proton exchange membrane for separating electrode chambers from each other, and electrolyte solution.

## 1.2 Objectives

1.2.1 To study the effect of benzyl alcohol flow rate on the percentage conversion and percentage selectivity of benzaldehyde.

1.2.2 To compare the effect of different surface morphologies of  $\text{TiO}_2$  films including compact film and mesoporous film on the conversion and selectivity of benzaldehyde.

### 1.3 Scopes of research

1.3.1 The synthesis of photoanode, TiO<sub>2</sub> film, was synthesized via sol-gel method. There are two different film morphologies including as follows.

1) Compact film: Titanium (IV) isopropoxide as a precursor was mixed with hydrochloric acid in ethanol solution at ambient conditions.

2) Mesoporous film: Titanium (IV) isopropoxide as a precursor was mixed with hydrochloric acid and Pluronic (P123) triblock copolymer in ethanol at ambient conditions.

After that, the prepared precursor solution was coated on fluorine-doped tin oxide (FTO) glass using convective deposition technique at 0.9 m/s deposition speed. The obtained films were characterized via following equipment.

- UV - Vis Spectrophotometer: To observe the absorption wavelength of film
- Scanning Electron Microscope: To examine surface morphology and measure film thickness
- X-ray diffraction: To verify phase formation of TiO<sub>2</sub> films

1.3.2 The operating condition of a continuous flow PEC reactor includes (i) different morphologies of TiO<sub>2</sub> films: compact and mesoporous films. (ii) flow rate via a syringe pump ranging from 0.05, 0.10, 0.15, and 0.20 ml/min. The UV lamp was used as a light source which illuminates UV light on the photoanode surface. The DC supplier was used to apply current density to both electrodes. The product composition was characterization via high performance liquid chromatography (HPLC) equipped with a C18 column. Feed streams contain 0.1 M sodium sulfate solution in the cathode channel and 0.1 M sodium sulfate solution with 0.02 M benzyl alcohol in the anode channel.

### 1.4 Expected Benefits

1.4.1 A continuous flow PEC reactor is designed and fabricated.

1.4.2 Effect of benzyl alcohol concentration and flow rate is studied with an achievement of high percentage conversion and percentage selectivity of benzaldehyde.

1.4.3 Effects of difference morphologies of photoanodes including compact TiO<sub>2</sub> film and mesoporous TiO<sub>2</sub> film on percentage conversion and percentage selectivity of benzaldehyde are compared.



## CHAPTER 2

### THEORY AND LITERATURE REVIEWS

This chapter describes the properties and conventional manufacturing of benzyl alcohol and benzaldehyde, theoretical background of photoelectrochemical (PEC) cells and fabrication of TiO<sub>2</sub> photoanode which is a key component in the PEC cell. The last section reviews alternative oxidation methods of benzaldehyde production from other previous work.

#### 2.1 Benzyl alcohol

Benzyl alcohol is an aromatic alcohol that can be obtained from natural ingredients such as peaches, apricots, cranberries, teas, and essential oils from hyacinth, ylang-ylang, and jasmine. However, the benzyl alcohol content derived from these plants is about 30 mg/kg which is quite low. The main source of benzyl alcohol production comes from petroleum-derived feedstocks which is the hydrolysis of benzyl chloride [8], as shown in **figure 2.1**.

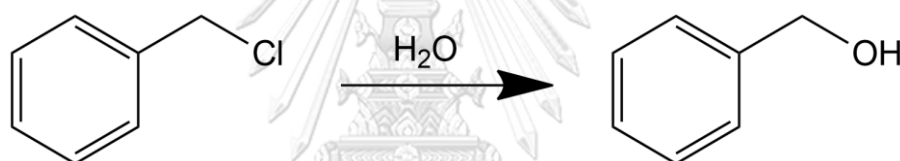


**Figure 2.1** Hydrolysis of benzyl chloride to benzyl alcohol

Benzyl alcohol has a sweet odor, bacteriostatic and antiseptic properties. It is always found in fragrances, cosmetic products, and food additives. shampoo, soaps, cleaners, and detergents. Another role of benzyl alcohol is an important precursor to generate other value-added chemicals including the synthesis of ester and essentially in an oxidation reaction to produce benzaldehyde or benzoic acid depending on the catalyst used. [9, 10]

#### 2.2 Benzaldehyde

Benzaldehyde is a colorless yellow liquid. The structure consists of a benzene ring and a formyl group which is the simplest aromatic aldehyde. In nature, benzaldehyde can be found in many plants such as almonds, cherries, and peaches in the form of glycoside. [11] Many industries require benzaldehyde as an ingredient or intermediate for their products including medicine, perfume, food, dye, and essentially production of several organic compounds. In 2022, the global value of benzaldehyde was about 214.8 million USD. According to the increasing demand for derivative compounds of benzaldehyde, including benzoic acid, cinnamic acid, and sodium benzoate, it was estimated to reach 291.4 million USD in 2028 with a compound annual

growth rate of 4.4%. [12] Moreover, the price is found as high as 70 USD/kg for a high purity (>99%) in 2023. [13]

The current production methods of benzaldehyde including hydrolysis of benzal chloride and air oxidation of toluene have a major drawback in terms of conversion, selectivity, energy efficiency, and waste emission. A selective oxidation of benzyl alcohol, on the other hand, gets more attention from many researchers as the best candidate method to solve the problem. [14]

### 2.2.1 Conventional method

#### 1. Hydrolysis of benzal chloride

Hydrolysis of benzal chloride is the oldest process for benzaldehyde production which is no longer used in the present day due to the waste emission and energy efficiency. Water and benzal chloride were changed into the gas phase using a vaporizer at 230°C. Then, the mixture was fed through a packed column containing activated carbon as a catalyst at 180°C. The outlet gas was cooled into liquid and the impurity was removed via extraction and distillation. [15] The reaction is shown in **figure 2.2**.



**Figure 2.2** Hydrolysis of benzal chloride to benzaldehyde.

#### 2 Air oxidation of toluene

Air oxidation of toluene is the main method for producing benzaldehyde because the production can be operated in either vapor or liquid phase. Mo, Fe, Co, Mn, and Ni are usually used as main catalysts together with Mg or copper oxide as a promoter to improve selectivity. The operating conditions are in the range of 100-500°C and 1-10 bar. The contact time must be optimized to maximize yield by preventing overoxidation. [15] The reaction is shown in **figure 2.3**.

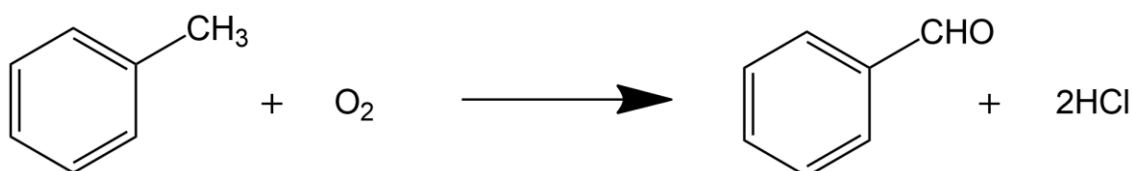


**Figure 2.3** Air oxidation of toluene to benzaldehyde.

### 2.2.2 Oxidation of benzyl alcohol

Oxidation of benzyl alcohol to benzaldehyde is a promising alternative method to produce benzaldehyde due to high conversion and selectivity compared to other processes. The

reaction is shown in **figure 2.4**. There are several oxidation methods to produce benzaldehyde. The most common is oxidation via noble metal catalyst, which is expensive. Some of them are toxic and essentially can cause overoxidation which decreases the selectivity of the product. Oxidation using electrochemical, photocatalysts, and photoelectrochemical are alternative ways to solve the problem.

In this study, the photoelectrochemical cell is chosen for oxidation of benzyl alcohol which is paired with a green hydrogen production. This approach has the advantages over the photocatalytic process including (1) The overcome of the applied voltage to prevent photogenerated charge recombination gives an improvement of product selectivity and (2) The separation of reduction and oxidation reaction provide a simple method to collect each product separately. [16]

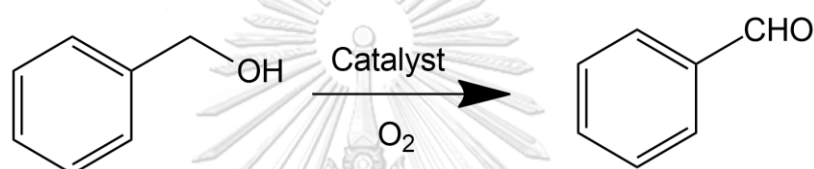


**Figure 2.4** Oxidation of benzyl alcohol.

### 2.3 Hydrogen production

Hydrogen is an energy carrier and clean sustainable fuel for the future due to its high energy density. However, the cleanness of production must be considered because most of conventional production processes consume high energy and cause an environmental impact. [17] The main raw materials for hydrogen production come from natural gas, oil, and coal, causing high emissions of CO<sub>2</sub> and burnout fossil fuels. So, alternative hydrogen production must be developed to solve this problem. The percentage of resources for hydrogen production is shown in **figure 2.5**.

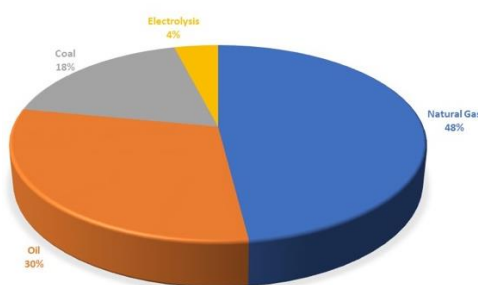


**Figure 2.5** Percentage of hydrogen production source [18]

#### 2.3.1 Steam reforming

Stream reforming is the most common process in hydrogen production. The reaction consists of hydrocarbon and steam to produce carbon monoxide and hydrogen gas. Natural gas is

a favored hydrocarbon reactant which mainly consists of methane, and undergoes the endothermic steam reforming reaction using Co-Ni as a catalyst at temperature of 700-100°C and pressure of 3-5°C, as shown in equation (1). If the product is contained more than 2000 ppm of CO, it is necessary to reduce to below 1000 ppm in a shift converter through a water gas shift reaction, as expressed in equation (2). [19] The overall process is shown in **figure 2.6**.

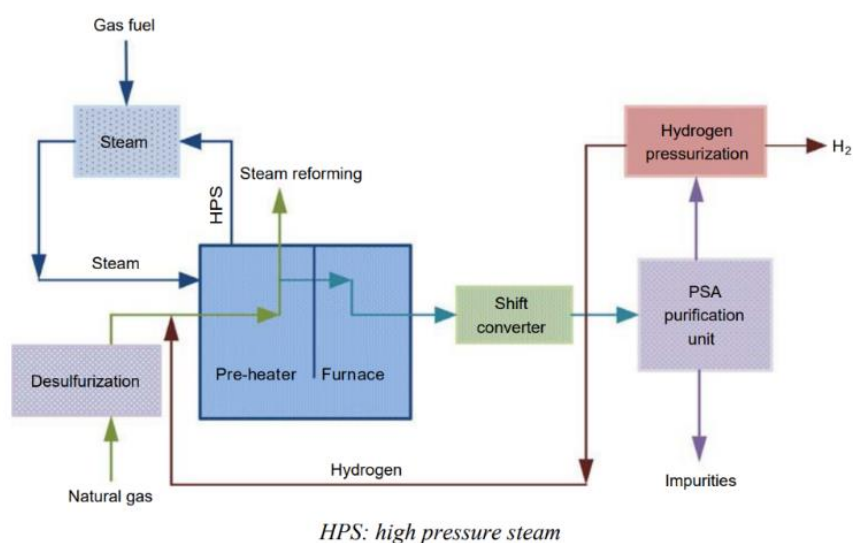
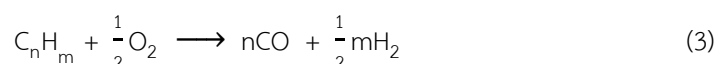


**Figure 2.6** Natural gas steam reforming process [19]

### 2.3.2 Partial oxidation

The partial oxidation process is preferred to produce hydrogen from heavy hydrocarbon due to a wide range of hydrocarbon reactants from methane to heavy fuel oil and coal. This process involves the combustion of hydrocarbon and partial oxygen using a transition-metal-based catalyst. The product contains hydrogen, carbon monoxide, and other partially oxidized species, as shown in equation (3). The benefit of this process is that it does not required any energy source because of a highly exothermic reaction. [20]



### 2.3.3 Coal gasification

Producing hydrogen from coal is the oldest method which is not favored in the present day because of the pollutant emission and high temperature required. The coal is converted into a gas phase by heating at least 900°C, then reacted with oxygen and steam at 857°C with a presence of catalysts such as nickel-based catalyst, or FeO-CrO<sub>2</sub>-ThO<sub>2</sub>, as shown in equation (4).

CO contained in the product is changed to CO<sub>2</sub> via water gas shift, as previously described in equation (2). Finally, the product is purified by the elimination of CO<sub>2</sub> using CaO. [19] The process is shown in **figure 2.7**.

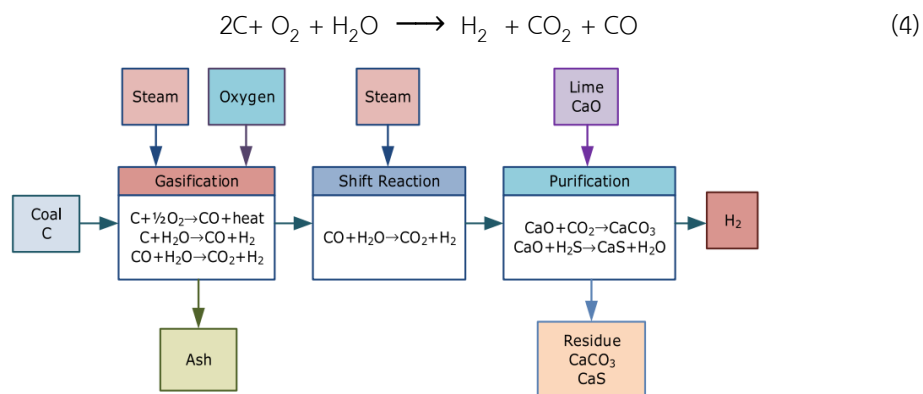


**Figure 2.7 Coal gasification process. [19]**

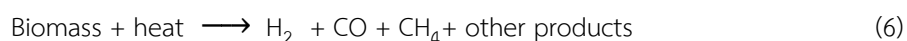
#### 2.3.4 Hydrogen production from biomass

Biomass is a renewable resource for energy production that comes from several ways including plants, animal materials, agricultural products, and other biological waste. Gasification and pyrolysis are the main processes for hydrogen production from biomass. Most of the products consist of CH<sub>4</sub> and CO, which can improve the hydrogen yield by steam reforming and water gas shift.

Biomass containing at least 35% moisture can be a source for the gasification process by gasifying with heat and steam at more than 1000 K to obtain syngas, methane, and charcoal, as shown in equation (5). [19]



While pyrolysis is composed of several reactions to form products in solid, liquid, and gas phases including biochar, bio-oil, methane, hydrogen, and carbon monoxide, as shown in equation (6). The operating temperature is a result of the composition. When the temperature exceeds 450°C, bio-oil mainly occurs, while biochar is required lower than 450°C. [20]



#### 2.3.5 Water splitting

Water is one of the abundant sources of hydrogen production due to the chemical reaction when hydrogen is used as a fuel. The combustion reaction with oxygen in the air generates water which is completely renewable. However, the major drawback is mainly

hydrogen production from water processes like electrolysis requires high energy input. An electrolysis system consists of an anode and cathode submerged in an electrolyte solution, while electricity is applied on both electrodes to stimulate the endothermic reaction. [19] In case of thermal cracking, it requires a temperature of at least 2500°C to decompose water into hydrogen and oxygen gas. However, the thermochemical cycles were developed to decrease the temperature required in thermal cracking to be lower than 1000°C by creating a closed loop to decompose water into hydrogen and oxygen using catalysts then separation to reuse the catalyst in the next cycles. [20]

#### 2.4 Photoelectrochemical cell

In a photoelectrochemical cell, the solar light is used to illuminate the system and then converted into electrical energy via a semiconduction photocatalyst in addition to an applied electrical energy to catalytic the reaction. The reaction is the combination of photocatalytic reaction and electrolytic reaction. The photoelectrochemical cell consists of one or two photoelectrodes as an anode and/or cathode submerged in an electrolyte which is a conductive solution for charge carrier from the photoelectrode to the counter electrode. The electrodes are connected to external bias for applied voltage and set separately in two chambers by proton exchange membrane (PEM) to allow only protons to pass through the system [21], as shown in **figure 2.8a**. There are three conventional types of photoelectrochemical cells, as shown in **figure 2.8b-c**. (1) n-type semiconductor at photoanode and a metal cathode. (2) p-type semiconductor at photocathode and a metal anode. (3) n-type semiconductor at photoanode and p-type semiconductor at photocathode. [3] The first developed photoelectrochemical cell is water splitting consisting of an n-type semiconductor as a photoanode and a metal as a cathode.

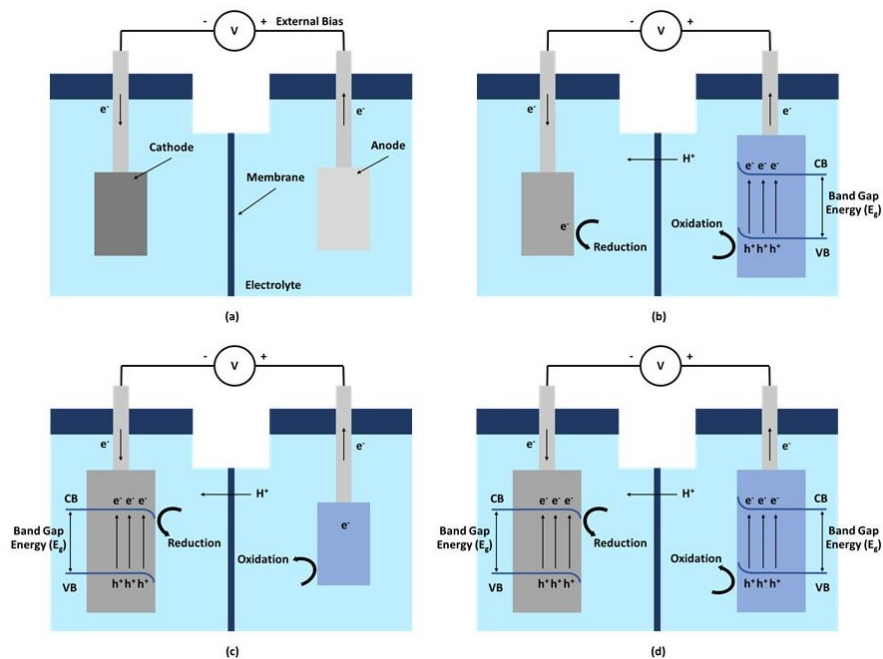
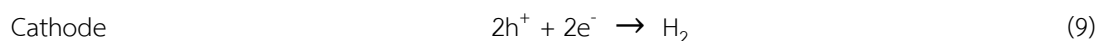
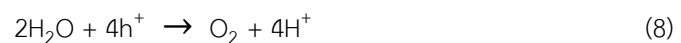
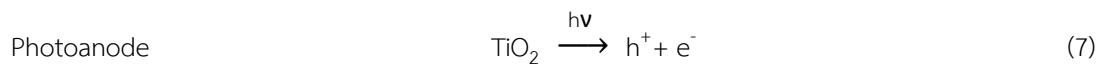


Figure 2.8 (a) Photoelectrochemical cell component. (b) n-type semiconductor photoelectrochemical cell. (c) n-type semiconductor photoelectrochemical cell. (d) Dual photoelectrochemical cell.

#### 2.4.1 Photoelectrochemical cell water splitting

In 1972, Fujishima and Honda successfully developed photoelectrochemical cell of water splitting for hydrogen production. The system consists of  $\text{TiO}_2$  photocatalyst as the photoanode and Pt as the cathode. From **figure 2.9**, when the light with higher energy than semiconductor band gap illuminates the photoanode ( $h\nu > E_g$ ), electrons ( $e^-$ ) at the valence band are excited and then moved to the conduction band, leaving holes ( $h^+$ ) at the valence band. Water at the anode side is oxidized by generated holes to produce oxygen and protons, as described in equations (7) to (8). The generated electrons transfer to the cathode side through an external wire, while the protons transfer through the membrane and then react with electrons to form hydrogen gas, as expressed in equations (9). [22]



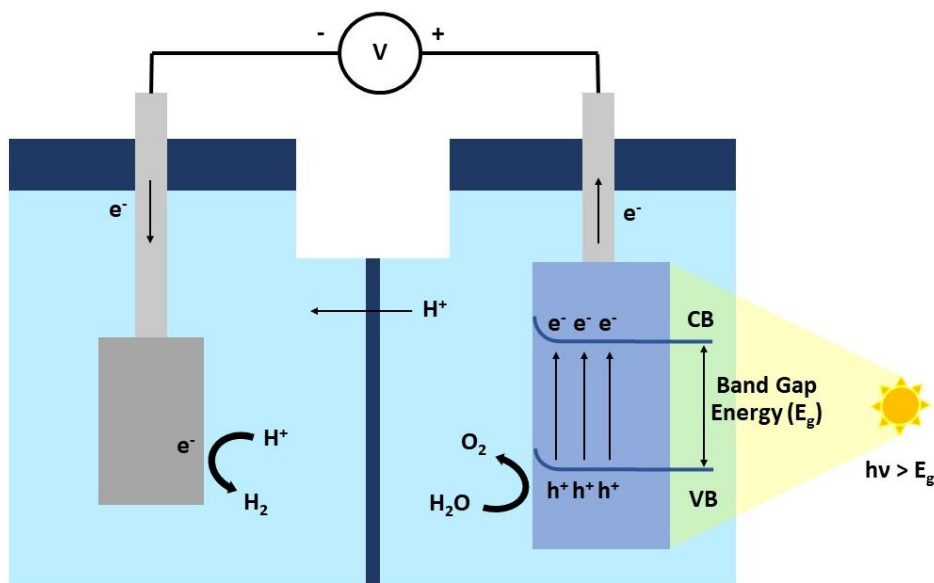
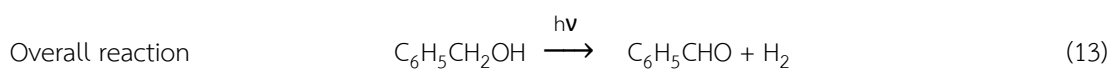
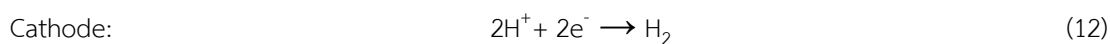
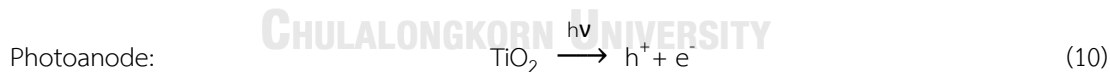


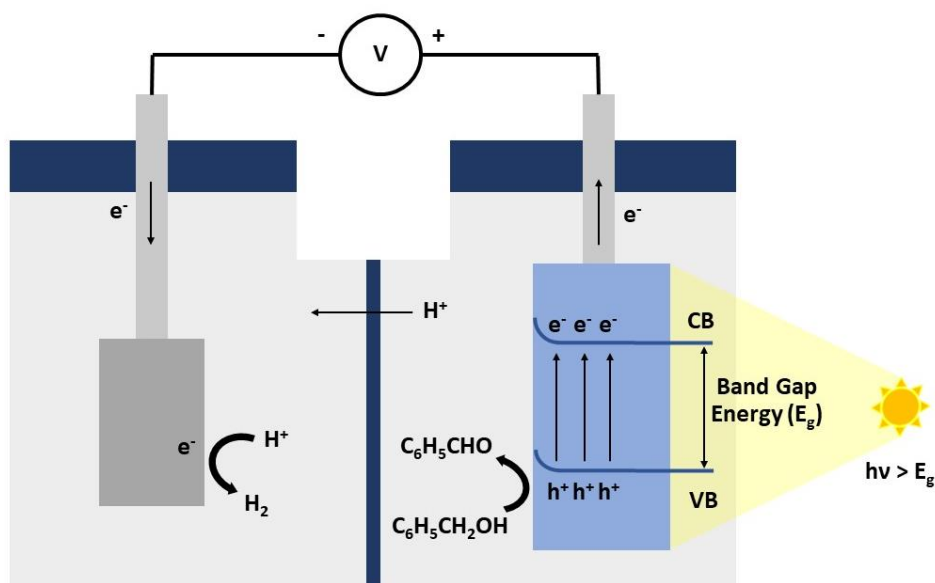
Figure 2.9 Schematic diagram of photoelectrochemical cell of water splitting.

#### 2.4.2 Photoelectrochemical cell for benzyl alcohol oxidation

The photoelectrochemical oxidation of organic compounds like benzyl alcohol was first developed to improve energy efficiency and the value of the product. The mechanism of photoelectrochemical oxidation of benzyl alcohol is shown in **figure 2.10**. In the beginning, the reaction is similar to water splitting. The difference is that benzyl alcohol which is in the anode side together with  $\text{Na}_2\text{SO}_4$  solution as an electrolyte is oxidized by generated holes in the stand of water and then generates benzaldehyde and proton, as described in equations (10) to (11). Then, the transferred electrons and protons combine to form hydrogen gas at the cathode, as described in equations (12). The overall reaction described in equations (13) [23]

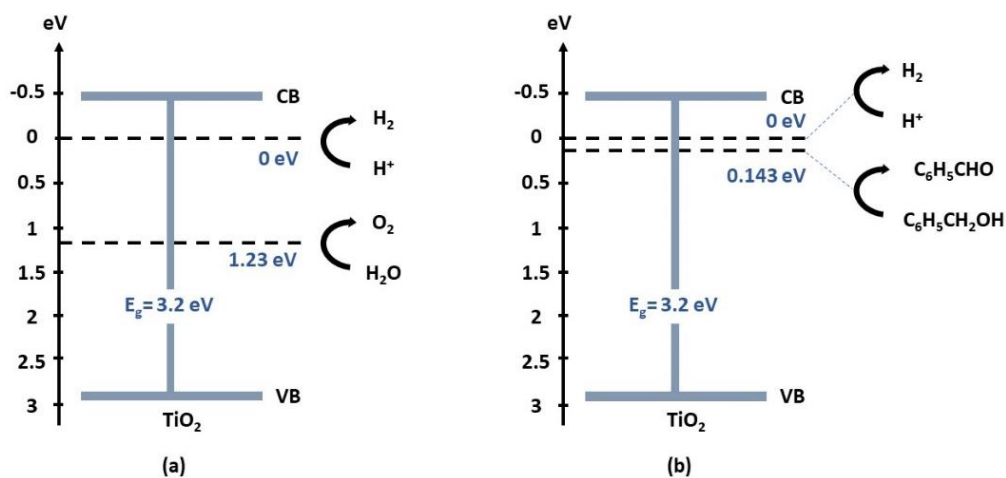






**Figure 2.10** Schematic diagram of photoelectrochemical oxidation of benzyl alcohol.

In order to select the suitable electrode material, the semiconductors must be considered in terms of the band edge position that can implement oxidation and reduction reaction of the system. In the case of water splitting, the valence band potential must be larger than 1.23 eV which is the redox potential of oxygen evolution reaction ( $O_2/H_2O$ ). While the conduction band potential must be lower than 0 eV which is the redox potential of hydrogen evolution reaction ( $H^+/H_2$ ). [24]  $TiO_2$  is the most widely studied and applied in the semiconductor field because of its properties for this purpose.  $TiO_2$  has a valence band potential of -0.4 eV and a conduction band potential of 2.8 eV, which comprehend both oxygen evolution and hydrogen evolution reactions. In the case of benzyl alcohol oxidation, the redox potential of benzyl alcohol oxidation to benzaldehyde is 0.143 eV [25] which is also in between of  $TiO_2$  band potential, as shown in **figure 2.11**.

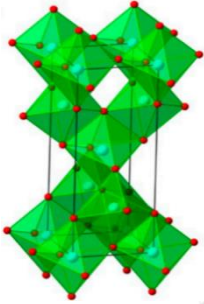
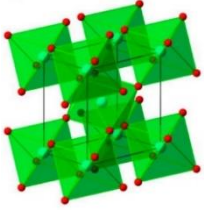
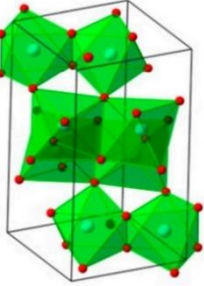


**Figure 2.11** (a) Band diagram of photoelectrochemical cell of water splitting. (b) Band diagram of photoelectrochemical cell of benzyl alcohol oxidation to benzaldehyde.

## 2.5 Titanium dioxide

Titanium dioxide (TiO<sub>2</sub>), also known as titanium (IV) oxide, is an n-type semiconductor that was first discovered in 1791 by William Gregor. [26] TiO<sub>2</sub> has been used in various fields of photocatalysis including water treatment, CO<sub>2</sub> conversion, organic degradation, and organic oxidation. It is also used in many industries such as food, cosmetics, and pigment because of its high physical and chemical properties, inexpensiveness, and non-toxicity. There are three phases of titanium dioxide which are mainly found including anatase, rutile, and brookite phases, their structures are as shown in **table 2.1**. The most stable phase is rutile but anatase has higher photovoltaic and photocatalytic properties due to the wider band gap energy. [27] However, the large band gap energy causes a major drawback for applications because TiO<sub>2</sub> can absorb only the ultraviolet (UV) region which is a small part of solar light. There are several methods to synthesize TiO<sub>2</sub> in form of film and nanoparticles.

Table 1 Physical properties and structure of TiO<sub>2</sub>

Properties	Crystalline phase			Ref.
	Anatase	Rutile	Brookite	
Structure				[28]
Unit cell	Tetragonal	Tetragonal	Orthorhombic	[29]
No. of TiO <sub>2</sub> /Unit cell	4	2	8	
Band gap (eV)	3.2	3.0	3.2-3.8	
Refractive index	2.49	2.61	2.58	
Density	4.26	3.84	4.11	

### 2.5.1 Synthesis of TiO<sub>2</sub> nanoparticles

#### 1. Sol-gel

Sol-gel is a wet chemical method along with precipitation and hydrothermal which is a popular process to synthesize nanomaterial due to the simplicity of equipment and effectiveness. The process starts with a hydrolysis reaction of organic metal or inorganic compound with alcohol or water. The hydrolysis reaction occurs along with polycondensation to form colloidal (sol). When hydrolysis and polycondensation occur, the network structure of titanium and oxide is formed (gel). [30] Then, the solvent is removed by evaporation and solid particles of TiO<sub>2</sub> is obtained. To fabricate TiO<sub>2</sub> as a thin film, the colloidal solution can be deposited on the substrate by a variety of deposition techniques, and then a thin liquid film is annealed to form a thin film, as shown in **figure 2.12**.

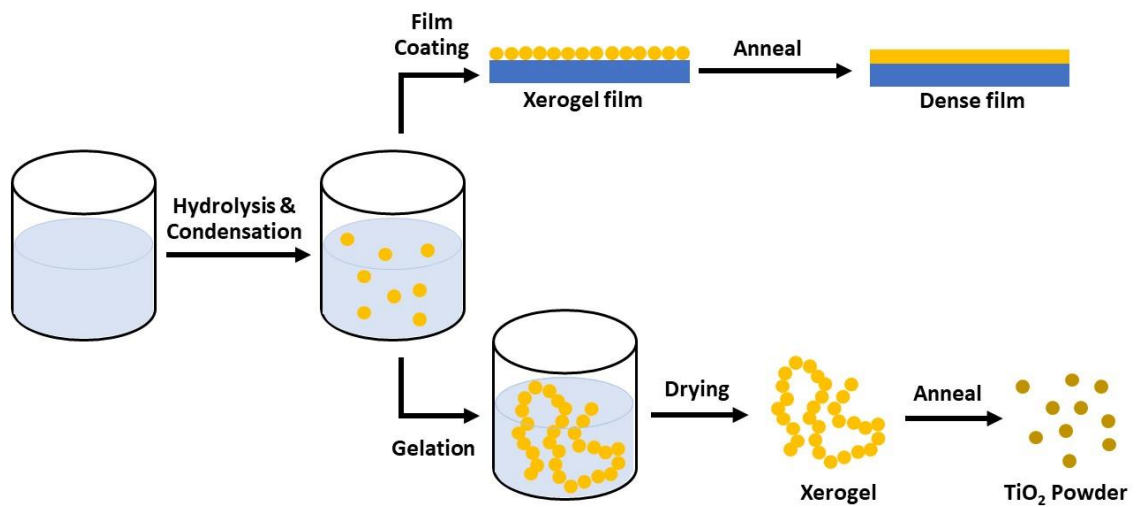


Figure 2.12 Schematic diagram of sol-gel method.

In this work,  $\text{TiO}_2$  anatase phase was synthesized via sol-gel method by using titanium (IV) isopropoxide as a precursor and ethanol as a solvent. The mechanism is shown in figure 2.13.

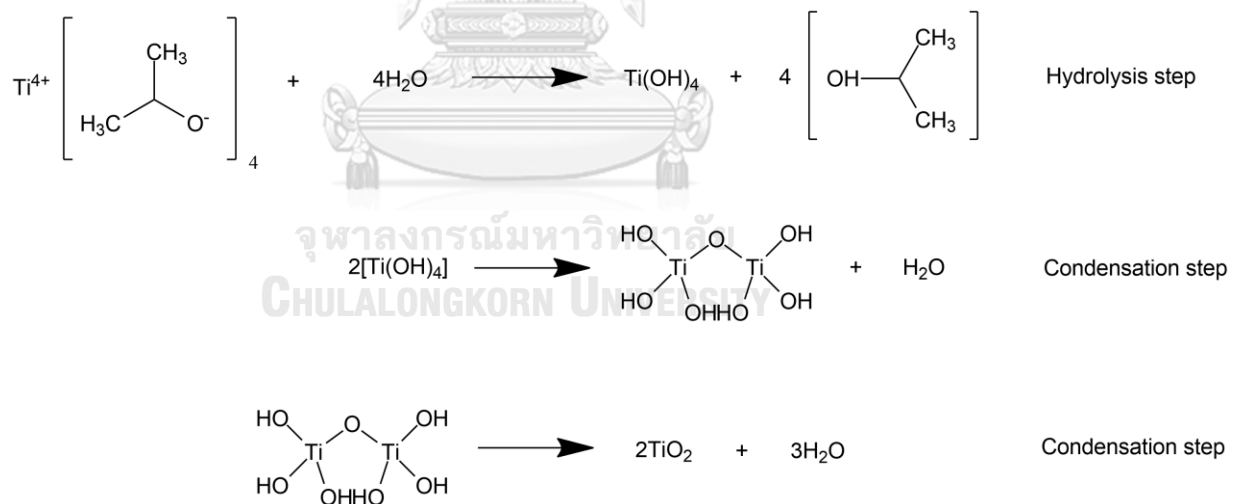


Figure 2.13 Mechanism of  $\text{TiO}_2$  synthesized via sol-gel method using TTIP.

## 2. Precipitation

Precipitation is a common technique for nanoparticle preparation. When the concentration of the substance exceeds its solubility in the solvent, the solid particle will be formed. The quality of the product depends on the concentration of precursor, reaction temperature, pH, and additive agent. The precipitation starts when the solution is saturated and the nucleus is begun to form in a liquid called “nucleation”. Then the nuclei grow bigger until

they exceed a critical radius. The smaller particle will likely be redissolved while the bigger ones continue to grow. Finally, the colloidal solution is obtained. [30]

### 3. Hydrothermal and solvothermal

Hydrothermal and solvothermal use high temperatures and pressure that excess boiling point of the solvent to increase the solubility and reactivity of metal salt and complex which badly in normal conditions. The difference between hydrothermal and solvothermal is the solvent in the process. Water is used as a solvent for hydrothermal, meanwhile solvothermal refers to a nonaqueous system. The method starts with solution configuration and aging before heating for material crystallization in a steel pressure vessel (autoclaves). The temperature can be operated up to 800°C depending on the reaction, while pressure depends on temperature. The product will be obtained after centrifuging, washing, and calcination. The schematic diagram of autoclave equipment is shown in **figure 2.14**. [31]

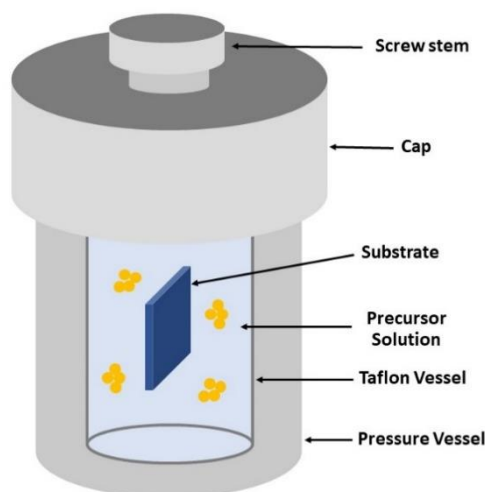


Figure 2.14 Schematic diagram of hydrothermal and solvothermal method.

### 4. Sonochemical method

Sonochemical is a nanomaterial synthesis method using ultrasonic waves to break chemical bonds and crystallization. The effect of the ultrasonic wave is called acoustic cavitation and consists of creation, growth, and collapse of the bubble in a very short time. First, the ultrasonic wave creates bubbles along with breaking of a chemical bond to form a cation, anion, and diffused vapor of solution. The generated vapor is diffused into the bubbles and then collapses. The temperature can be up to 5000 K while the pressure can reach 500 atm at the bubble surface in a very short time. This causes the local melting of suspended in solution then crystallization occurs. [32]

Dimas et al. synthesized TiO<sub>2</sub> anatase phase via sonochemical method and followed by hydrothermal NaOH treating from titanium isopropoxide in methanol and acetone solution. The 50 kHz ultrasonic was applied to the solution for 50 min and dried at 80°C. The as-prepared solution was treated hydrothermally with NaOH at 110°C for 24 h. Then the solution was stirred at 50°C and the TiO<sub>2</sub> anatase phase was obtained with 5.2 ± 1.5 nm of crystallite size. [33]

## 5. Microwave irradiation

Microwave is an electromagnetic wave with a frequency between 300 MHz to 300 GHz but the range of 900 MHz to 2.4 GHz can only be used for heating. In general, when the microwave irradiates the solution, most of the wave can pass through the interior to supply electromagnetic energy and a reflection of the rest. The electromagnetic energy will be converted into heat energy. The capability for conversion is proportional to the dielectric constant of the material. The major drawback of microwave irradiation is the instability of the electromagnetic field in a microwave oven. Therefore, this causes non-uniform heating in the material. [30]

### 2.5.2 Thin film deposition of TiO<sub>2</sub>

In order to obtain photoelectrode, the photocatalyst needs to be deposited on the transparent conductive substrate via the thin film deposition method which can be separated into 3 major techniques including chemical vapor deposition, physical vapor deposition, and solution-based chemical deposition, as shown in **figure 2.15**. [34]

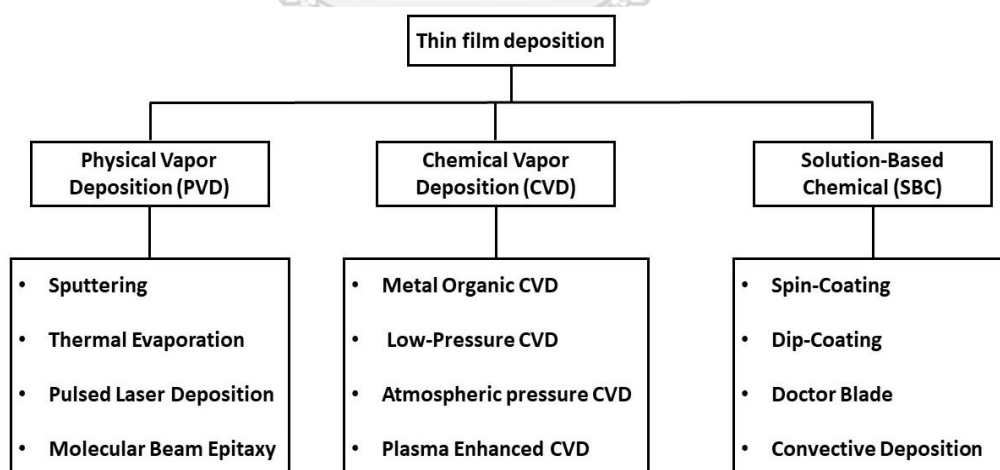


**Figure 2.15** Classification of thin film deposition technique.

### 1. Chemical vapor deposition (CVD)

Chemical vapor deposition is a widely used method in the thin-film coating of semiconductor material field due to high deposition rate, producing a thick film, and can operate

with various sizes of substrate. The process starts with the vapor phase of the precursor fed into the reactor chamber containing a substrate via an inert carrier gas. The gas moves onto the substrate surface and is then absorbed on the surface, where chemical reaction occurs. Finally, by-product gas from the reaction is desorbed and taken out of the reactor. The schematic diagram of chemical vapor deposition is shown in **figure 2.16**. The disadvantage of this method is the required high temperature, toxicity of the precursor or excess by-product, and complex system. [35]

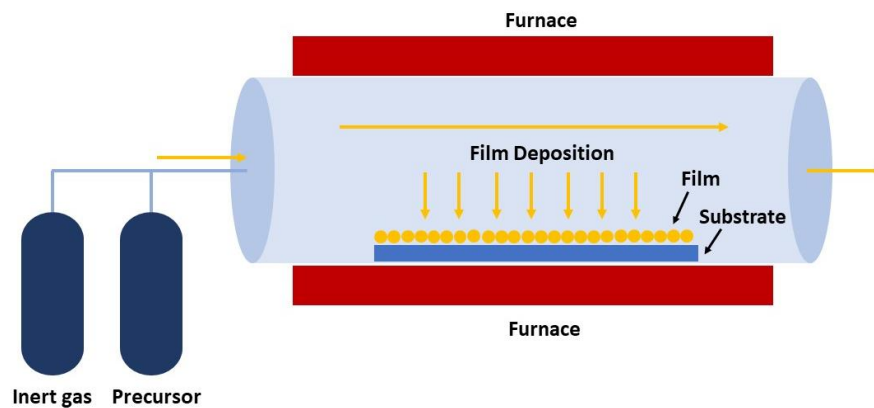


**Figure 2.16** Schematic diagram of chemical vapor deposition.

## 2. Physical vapor deposition (PVD)

Physical vapor deposition is a method using the vapor phase to deposit on the substrate which is similar to chemical vapor deposition. The liquid or solid phase of the source material in the vacuum reactor changes into vapor via various methods such as thermal evaporation or sputtering. The vapor transfer at the atomic level to the conductive substrate. Then the vapor is condensed on the surface of the substrate and the thin film is formed. The schematic diagram of physical vapor deposition is shown in **figure 2.17**. This method is safer than chemical vapor deposition, however, the deposition rate is quite low and the film is thinner compared to chemical vapor deposition. [36]

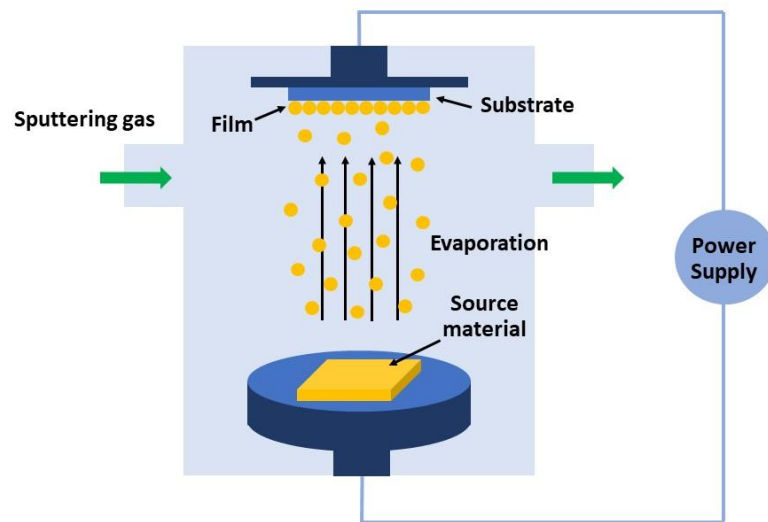


Figure 2.17 Schematic diagram of physical vapor deposition

### 3. Wet chemical method

#### a) Spin-coating

Spin-coating method creates a thin film by rotation of the symmetric substrate. The centrifugal force distributes the precursor to generate a uniform film along the surface of the substrate, usually used in electronic parts and antireflection coating. Normally, the film has a thickness in a range of 1-10  $\mu\text{m}$  which mainly depends on spinning velocity. Other factors that affect film thickness are spinning time, surface tension and viscosity of the solution. The method starts with dropping the precursor solution on the substrate, followed by spin-up and spin-off in sequence. The solvent is evaporated during the process, as shown in **figure 2.18**. The advantage of this method is that a small amount of reagents is required for film deposition and it is very fast to operate. However, this method requires a small size of substrates and must be in a symmetric shape. [30]



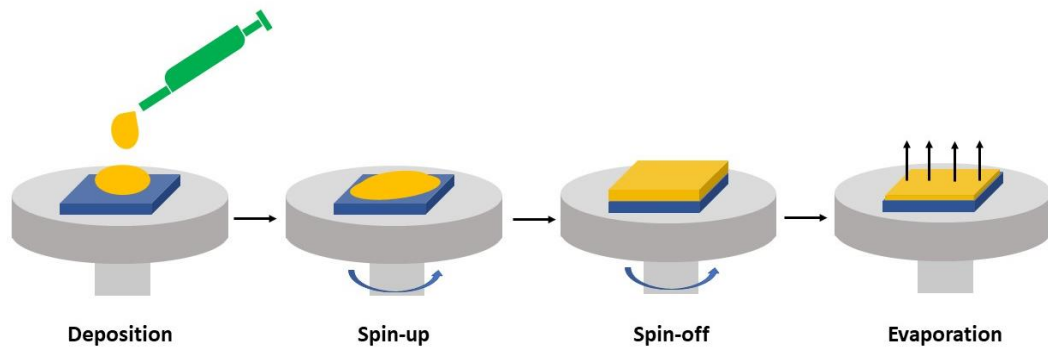


Figure 2.18 Procedure of spin-coating methods.

b) Dip-coating

Dip-coating employs a certain viscosity of solution for film deposition. First, the substrate is submerged into the precursor solution, and then withdrawn at a constant velocity followed by solvent removal via gravitational force and evaporation, as shown in **figure 2.19**. The film thickness is dependent on solution viscosity and withdrawal rate. This method is simple to set up, low cost, and essentially various shape of substrates can be used. The major drawback is that it requires a lot of solution and the overall surface of substrate must be coated. [35]

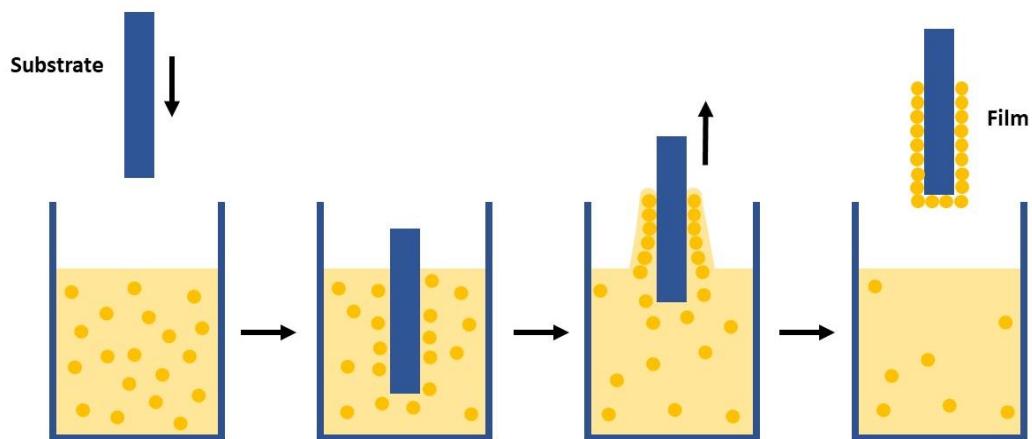


Figure 2.19 Procedure of dip-coating method.

c) Doctor blade

The doctor blade is a technique to form a uniform thin film that can control film thickness appropriately. The doctor blade consists of a platform for placing the substrate and a moving blade above. The blade is set a little behind a substrate. The precursor solution is injected in between. After that, the blade will move at constant velocity to cover the substrate with a film as shown in **figure 2.20**. [37]

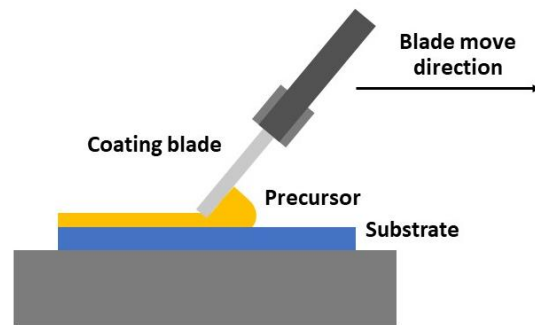


Figure 2.20 Schematic diagram of doctor blade.

d) Convective deposition

Convective deposition is an alternative coating process for large-scale flat plate substrate in a nanometer-scale film. The equipment consists of a moving platform and a static deposition blade. First, the precursor solution is injected between the substrate which is placed on the platform, and the deposition blade, followed by moving of the platform. The capillary force causes deposition of colloidal on the substrate along the way together with the evaporation of solvent via driven flow. The film thickness mainly depends on deposition speed and concentration of precursor. N. Khothong et al. found that high deposition velocity obtains more film uniformity and thickness because higher velocity causes a high viscous force which pulls more colloidal particles to deposit on the substrate. The schematic diagram of convective deposition is shown in figure 2.21. [38]

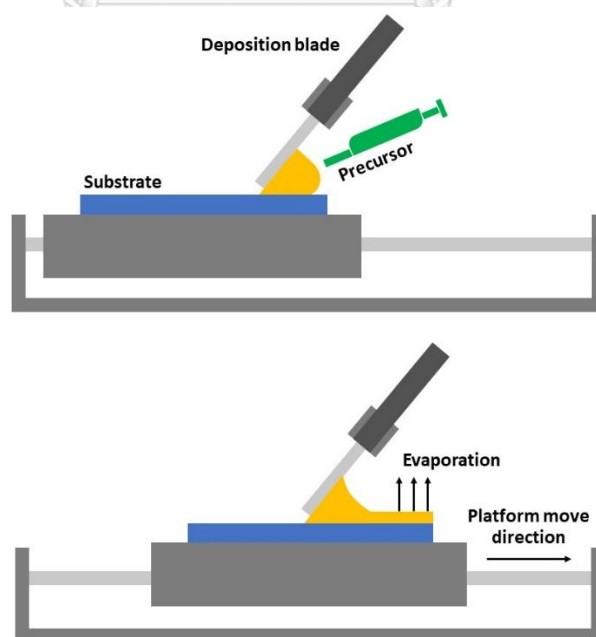


Figure 2.21 Schematic diagram of a convective deposition.

## 2.6 Literature review

The following section provides the previous related research of selective oxidation of benzyl alcohol. A summary table is shown in **table 2.2**.

**Table 2 Literature review summary**

Process	Material	Electrolyte	System	Result	Ref.
Photo-electrocatalytic	Anode: Au/TiO <sub>2</sub> NTPC Cathode: C/Cu <sub>2</sub> O NWAs	Na <sub>2</sub> SO <sub>4</sub>	Conventional three-electrode system	84.68% BA conversion 99% BD selectivity	[5]
	Anode: Bi <sub>2</sub> MoO <sub>6</sub> @TiO <sub>2</sub> NTA Cathode: C/Cu <sub>2</sub> O NW	Na <sub>2</sub> SO <sub>4</sub>	Conventional three-electrode system	67.4% BA conversion 98.6% BD selectivity	[39]
Electrocatalytic	Anode: Platinum Cathode: Platinum	Deionized water	Glass cell	97% BD yield	[40]
	Anode: Carbon felt Cathode: Carbon felt	Et <sub>4</sub> NClO <sub>4</sub> and acetonitrile	Batch system at ambient condition	94% BD yield	[41]
Photocatalytic	TiO <sub>2</sub> /Ti <sub>3</sub> C <sub>2</sub>	-	Quartz reaction Vessel at 15°C	97% BA conversion 98% BD selectivity	[42]
	Cu@NALC/TiO <sub>2</sub> /AC	-	Batch system	100% BA conversion 99% BD selectivity	[43]
	Rutile TiO <sub>2</sub> nanorods	-	Batch system	99% BD selectivity	[44]
Catalytic	Cobalt-based catalyst	-	Batch system	80% BA conversion 95% BD selectivity	[45]
	Cobalt propylene	-	Membrane microchannel reactor	88% BA conversion 91% BD selectivity	[46]
Simulation of continuous flow	Anode: Photocatalyst with golden mesh Cathode: Metal	Water	Oval shape continuous flow reactor	Gas production is increase due to the increasing of current density	[47]
	Anode: Photocatalyst Cathode: Metal	Water	Continuous flow reactor	High gas concentration at electrolyte-electrode interface	[48]
	Anode: Photocatalyst Cathode: Pt-Ti	Water	Flat plate continuous flow reactor	The increasing of electrolyte flow rate can minimize saturated oxygen generation	[44]

### 2.6.1 Photo-electrocatalytic

Z. Wu et al. (2017) studied the oxidation of benzyl alcohol in a Z-scheme type solar-driven dual photoelectrode photoelectrochemical cell using Au/TiO<sub>2</sub> nanotube photonic catalyst (NTPC) as a photoanode paired with C/Cu<sub>2</sub>O nanowire arrays (NWAs) as a photocathode, and Na<sub>2</sub>SO<sub>4</sub> as an electrolyte. The anode and cathode chambers were separated with Nafion 117 membrane, and each side was illuminated with 300 W xenon lamps. Au/TiO<sub>2</sub> (NTPC) was prepared via two-step electrochemical anodization of Ti-Au alloy foil with a Pt cathode in ethylene glycol solution. Besides C/Cu<sub>2</sub>O (NWAs) were also prepared via electrochemical anodization using a copper mesh with Pt cathode in NaOH solution. The result shows the percentage conversion of benzyl alcohol of 84.68%, and the selectivity of benzaldehyde of more than 99%. [5]

Z. Zhou et al. (2021) enhanced hydrogen production by using the oxidation of benzyl alcohol which is more economical than oxygen evolution reaction. A Bi<sub>2</sub>MoO<sub>6</sub>@TiO<sub>2</sub> nanotube arrays was chosen as a photoanode paired with C/Cu<sub>2</sub>O as a photocathode. The photoanode was synthesized via a sol-gel method by mixing Bi(NO<sub>3</sub>)<sub>3</sub>·5H<sub>2</sub>O with Na<sub>2</sub>MoO<sub>4</sub>·2H<sub>2</sub>O in an ethylene glycol solution. Finally, the reaction occurred under the solvothermal method with TiO<sub>2</sub> nanotube arrays in an autoclave. An electrochemical anodization was used for the synthesis of C/Cu<sub>2</sub>O photocathode by anodized copper mesh in a NaOH solution via a conventional three-electrode system. The photoelectrochemical reaction was studied in a double-chamber photoelectrochemical quartz reactor which was separated each chamber with Nafion 117 proton exchange membrane. A 300 W xenon lamp with AM 1.5 filter was used as a light source for both sides. Benzaldehyde selectivity was found at 98.6% with 67.4% conversion of benzyl alcohol. [39]

### 2.6.2 Electrocatalytic

G. Susila et al. (2022) studied the production of benzaldehyde by electrochemical oxidation of benzyl alcohol using potassium iodate via a biphasic electrolysis technique. The reaction occurred in a glass cell in which platinum was used as an anode and cathode and deionized water as an electrolyte. Briefly, benzyl alcohol, chloroform, and potassium iodate were added into a glass cell. The aqueous was separated into two layers of liquid. The upper layer consisted of potassium iodate as a mediator, while the lower one contained benzyl alcohol which was converted into benzaldehyde. The benzaldehyde product was found at 97% yield. [40]

G. Horiguchi et al. (2022) developed a linear paired electrolysis system to improve the production of benzaldehyde via direct oxidation at the anode and indirect oxidation at the

cathode. The system consisted of tetraethylammonium perchlorate ( $\text{Et}_4\text{NClO}_4$ ) and acetonitrile aqueous solution as an electrolyte which was carried out with carbon felt as the anode and various metals at the cathode. At the anode, water is split into protons ( $\text{H}^+$ ), electrons ( $\text{e}^-$ ), and oxygen gas. Benzyl alcohol was oxidized by oxygen to form benzaldehyde. The generated electrons transferred to the cathode side via external bias and then reacted with protons to form hydrogen gas, while oxygen generated oxidizing reactive oxygen species (ROS) via a reduction reaction. The remaining benzyl alcohol was oxidized by ROS, then the benzaldehyde was obtained, as shown in **figure 2.22**. The optimal cathode from the experiment was carbon felt which can obtain benzaldehyde as high as 94% yield and current efficiency of 146%. [41]

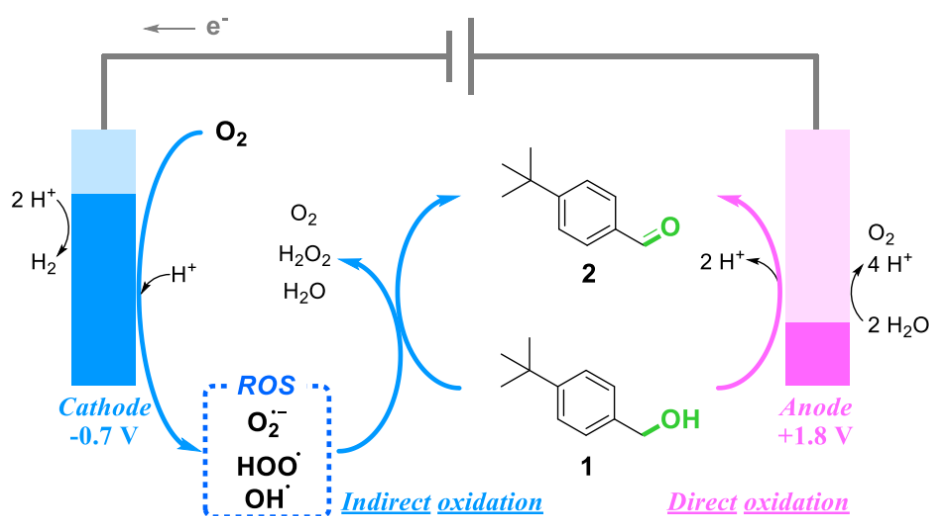


Figure 2.22 Proposed mechanism of benzyl alcohol oxidation via linear paired electrolysis.

[41]

### 2.6.3 Photocatalytic

X. Bao et al. (2021) found that  $\text{Ti}_3\text{C}_2$  can stimulate oxygen species to reduce  $\text{Ti}^{3+}$  into  $\text{TiO}_2$ . The formation of  $\text{TiO}_2/\text{Ti}_3\text{C}_2$  composite by calcination greatly improves photocatalyst properties of  $\text{TiO}_2$  during photocatalysis oxidation of benzyl alcohol to benzaldehyde by increasing active intermediate production and preventing overoxidation reaction, which promotes benzaldehyde selectivity. The method to synthesize composite photocatalyst starts with  $\text{Ti}_3\text{C}_2$  preparation by slowly adding HF into  $\text{Ti}_3\text{AlC}_2$  powder to remove Al. Then, the as-prepared powder was calcined and  $\text{TiO}_2/\text{Ti}_3\text{C}_2$  formed. The photocatalytic properties were tested in a quartz vessel by suspending  $\text{TiO}_2/\text{Ti}_3\text{C}_2$  in n-Hexane solution using a 300 W xenon lamp as a light source. The reaction was operated for 5 h. The optimal condition of the composite showed 97% benzyl alcohol conversion and 98% benzaldehyde selectivity. [42]

M. Farrag et al. (2020) successfully improved the photocatalyst efficiency of  $\text{TiO}_2$  by synthesis of copper clusters/titanium dioxide/activated carbon nanocomposite ( $\text{Cu@NALC/TiO}_2/\text{AC}$ ).  $\text{Cu@NALC}$  can enhance light absorption in the wavelength at 400-700 nm. The synthesis of  $\text{Cu@NALC/TiO}_2/\text{AC}$  nanocomposite consisted of 3 steps. First,  $\text{Cu@NALC}$  was prepared from mixing N-acetyl-L-cysteine, copper chloride, and distilled water. Then,  $\text{NaBH}_4$  was dropwise into the as-prepared mixture to reduce copper salt and grow of nanoclusters. Second, activated carbon was suspended in water before being added with  $\text{TiO}_2$  aqueous dropwise. The suspension was filtered and dried to obtain  $\text{TiO}_2/\text{AC}$ . Finally, the material from the previous steps was mixed in an aqueous solution, then evaporated the solvent.  $\text{Cu@NALC/TiO}_2/\text{AC}$  nanocomposite was obtained. The photocatalytic oxidation was performed in a 50 ml beaker with acetonitrile as a solvent. An Oriel Sol2A class ABA solar simulator which can illuminate a  $1000 \text{ W/m}^2$  was used as a light source. After 6 h of reaction, they achieved 100% conversion of benzyl alcohol and 99% selectivity of benzaldehyde. [43]

C. Li et al. (2011) synthesized single crystalline rutile  $\text{TiO}_2$  nanorods to oxidize benzyl alcohol to benzaldehyde via the illumination of visible light. The photocatalyst was prepared via hydrothermal reaction using rutile  $\text{TiO}_2$  nanorods as substrate. To prepare the catalyst, polyvinylpyrrolidone was dissolved in ethanol and mixed with  $\text{Ti}(\text{OBU})_4$  and acetic acid then performed electrospinning process to obtain rutile  $\text{TiO}_2$  nanofiber.  $\text{Ti}(\text{OBU})_4$  mixed with chloric solution and added as prepared rutile  $\text{TiO}_2$ . The suspended solution was operated a hydrothermal reaction in an autoclave at  $150^\circ\text{C}$  and varied reaction time from 4 to 24 hr. The photocatalytic reaction is performed in acetonitrile with magnetic stirring and the irradiation of xenon lamp with UV cut off as a visible light source. The optimal reaction time of photocatalyst is 8 hr of hydrothermal reaction time which can perform 99% benzaldehyde selectivity. [44]

#### 2.6.4 Catalytic

M. Lu et al. (2021) compared a cobalt-based catalyst from different synthesis methods over selective oxidation of benzyl alcohol using a three-neck glass flask that contains N, N dimethylformamide as a medium together with benzyl alcohol and a selected catalyst including  $\text{Co@CN}$  and  $\text{CoOx}$ . A cobalt-based zeolitic imidazolate framework (ZIF-67) was used as a precursor. For  $\text{Co@CN}$ , ZIF-67 was pyrolyzed with a continuous flow of argon gas at  $600\text{-}900^\circ\text{C}$  while  $\text{CoOx}$  was prepared by calcination of ZIF-67 at  $500^\circ\text{C}$ . The  $\text{Co@CN}$  shows a better activity over  $\text{CoOx}$  which can perform 80% conversion and 95% selectivity. Moreover,  $\text{Co@CN}$  also showed high stability due to the stable result after 4 cycles of reaction. [45]

Q. Han et al. (2021) studied the aerobic oxidation of benzyl alcohol to benzaldehyde via a membrane microchannel reactor using cobalt propylene as a catalyst. The schematic diagram

of the system is shown in **figure 2.23**. In brief, the first stream contains benzyl alcohol, 1,2-dichloroethane (DCE), and cobalt propylene. The second stream contains isobutyraldehyde and DCE. Both streams are mixed by T-mixer before feeding into the membrane microchannel reactor. The reactor consists of a two-phase channel. The inner pipe is for a liquid phase while the outer is for a gas phase, separated by a semipermeable membrane. The product was separated by a gas-liquid separator before being analyzed. The optimal condition was found at 0.27 mmol/L of cobalt propylene and 0.92 mol/L of isobutyraldehyde which obtained 88% conversion and 91% benzaldehyde selectivity in 6.5 min. [46]

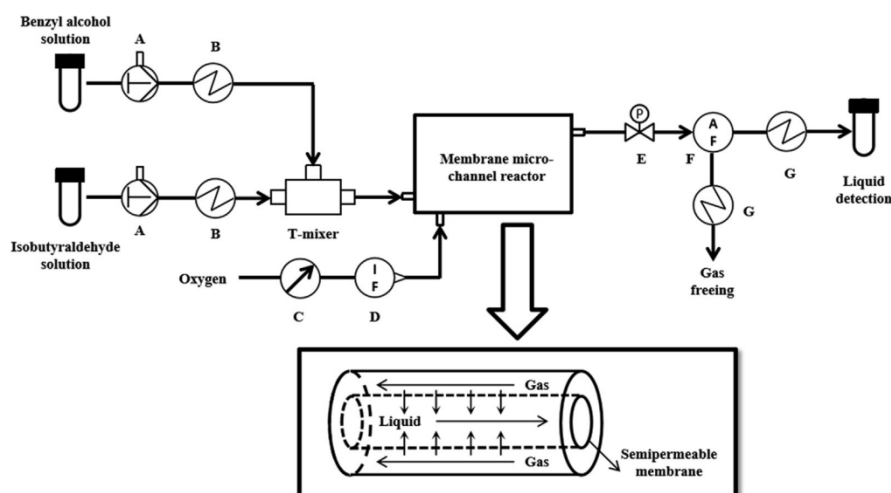


Figure 2.23 Schematic diagram of membrane microchannel reactor. A: Pump, B: Preheater, C: Gas pressure gauge, D: mass flow controller, E: backpressure valve, F: Gas-liquid separator, G: Condenser [46]

### 2.6.5 Simulation of photoelectrochemical cell

F. Farivar et al (2015) developed a continuous flow photoelectrochemical reactor water splitting via COMSOL Multiphysics software. They aimed to achieve a uniform flow with minimum recirculation and dead zones inside the chamber. After 20 configurations, they found an oval shape chamber that distributed the fluid flow by a series of pines at the inlet is the best design to generate a uniform flow along the reactor, as shown in **figure 2.24**. At the center of the photoanode, they found a huge potential drop due to a transparent layer of a substrate. To solve this problem, a golden mesh was used to increase the conductivity and found significantly decreased of potential drop from 25% to 6%. The result shows the amount of hydrogen and oxygen production increase with the increase of current density. [47]

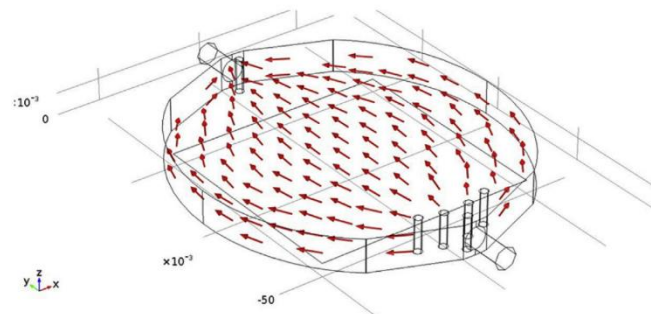


Figure 2.24 Photoelectrochemical chamber flow distribution. [47]

F. Njoka et al. (2017) simulated a 2-D photoelectrochemical reactor model was simulated for hydrogen production consisting of five domains including cathode, anode, electrolyte at cathode and anode, and ion-permeable membrane. The simulation focused on (1) the interface of electrode and electrolyte to acknowledge the transport phenomena and minimized the cost efficiency, and (2) the proton dissociation and the movement from anolyte to catholyte which is separated by a membrane to prevent product losses and danger under normal condition due to the recombination of hydrogen and oxygen. The result shows a gas production increase due to the increase of current density and a high concentration of gas production at the electrode which is wider along the reaction way, as shown in **figure 2.25**. [48]

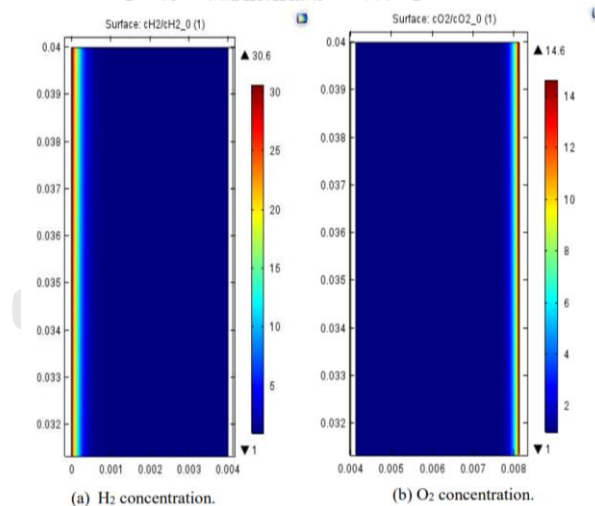


Figure 2.25 Hydrogen and oxygen concentration profile in photoelectrochemical cell [48]

C. Carver et al. (2012) modeled a flat plate continuous flow photoelectrochemical reactor for hydrogen production using COMSOL Multiphysics software, as shown in **figure 2.26**. Two major issues in photoelectrochemical cells were studied including current density distribution which decreased with the distance due to the poor conductivity of the conductive substrate, and the formation of oxygen gas bubbles. The formation of oxygen gas bubbles increased resistance at the covered electrode and decreased light adsorption due to the



reflection, resulting in a decrease in current densities to the formation bubble and making low productivity. The result showed the formation of bubbles at a current density of  $2\text{--}3\text{ A/m}^2$  which is quite low. Increasing electrolyte flow rate can decrease this problem. However, this causes a recirculation of bubbles at the corners, as shown in **figure 2.27**. [49]

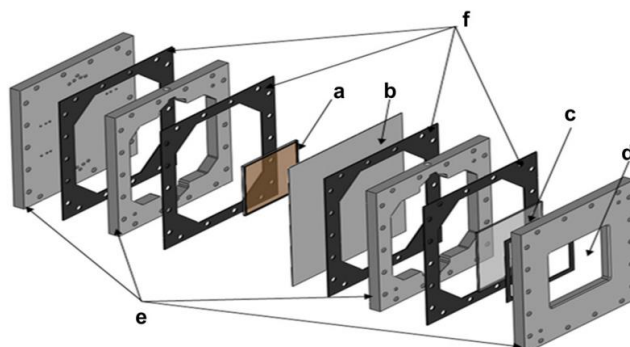


Figure 2.26 Flat plate continuous flow photoelectrochemical reactor consist of a) Anode, b) Nafion membrane, c) Platinized-Titanium cathode, d) Quartz window, e) Body plate, f) nitrile gaskets. [49]

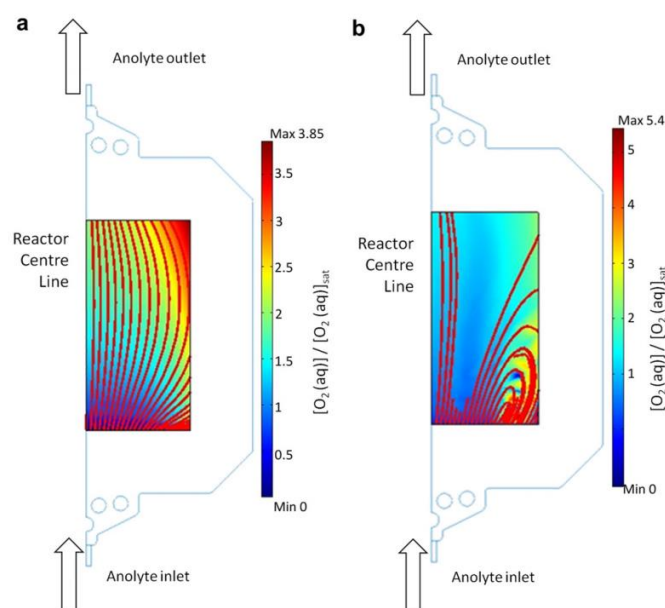


Figure 2.27 Effect of electrolyte flow rate on development of  $\text{O}_2$  saturation in the electrolyte a)  $6 \times 10^{-5}\text{ m}^3/\text{min}$ , b)  $15 \times 10^{-5}\text{ m}^3/\text{min}$ . [49]

#### 2.6.6 Literature review summary

Based on the literature reviews, there are several methods available for converting benzyl alcohol to benzaldehyde. These methods include photo-electrocatalytic, electrocatalytic, photocatalytic, and catalytic reactions. Each utilized different types of material to catalyze the reaction. In the case of photo-electrocatalytic and electrocatalytic reactions, a large-scale material or a film-coated catalyst is typically used, while homogeneous or nanoparticle catalysts

are preferred for other methods. According to the previous studies, the conversion of benzyl alcohol to benzaldehyde is high with good selectivity, but the reaction time is relatively long, typically more than 4 hours in batch-type reactors. However, recent research by Q. Han et al. (2021) using a continuous flow reactor, a membrane microchannel reactor, has demonstrated a significant improvement in reaction time, taking only 6.5 minutes. This is because continuous flow microreactors have several advantages, such as laminar flow, well-mixing, a high driving force of mass and heat transfer, and a high surface to volume ratio [50]. These advantages improve the overall process performance. In terms of economics, photoelectrochemical methods have an advantage over other methods due to their energy efficiency by assisting solar energy, and simultaneously offering a potential to generate hydrogen which is a valuable product for sustainable fuel. However, the formation of bubbles gas in the reactor and the decreasing current density along the electrode are the major problems that must be considered to improve the efficiency of the production. Numerous researchers have studied continuous-flow photoelectrochemical cells. Some have investigated by simulations, while some have conducted experiments. To the best of our knowledge, so far there has no reports on a fabrication of continuous flow PEC reactor for photooxidation of benzyl alcohol in a large scale.

## CHAPTER 3

### METHODOLOGY

#### 3.1 Chemicals and Equipment

##### 3.1.1 Chemicals

1. Deionized water (DI water)
2. Ethyl alcohol ( $C_2H_5OH$ , >99.9%, Quality Reagent Chemical)
3. Isopropyl alcohol ( $C_3H_7OH$ , CARLO ERBA Reagents)
4. Pluronic (P123, Sigma Aldrich)
5. Titanium (IV) isopropoxide ( $Ti[OCH(CH_3)_2]_4$ , >98%, Thermo Scientific)
6. Hydrochloric acid (HCl, 37%, Quality Reagent Chemical)
7. Hydrogen peroxide ( $H_2O_2$ , 30%, CARLO ERBA Reagents)
8. Benzyl alcohol ( $C_6H_5CH_2OH$ , >99%, Sigma Aldrich)
9. Sodium sulfate ( $Na_2SO_4$ , 98%, LOBA CHEMIE)

##### 3.1.2 Equipment

1. Hot plate stirrer
2. Ultrasonicator
3. UV-ozone
4. Convective deposition machine
5. Furnace
6. Syringe pump
7. DC supplier
8. UV lamp 100 W
9. Electrochemical H-cell
10. UV-vis spectrophotometer
11. Scanning electron microscope
12. X-ray diffraction
13. High-performance liquid chromatography

## 3.2 Experimental

### 3.2.1 Synthesis of TiO<sub>2</sub> thin film photoanode

#### 1. Substrate preparation

Fluorine-doped tin oxide (FTO) glasses, used as a substrate for photoanode, were cut into 4 × 8 cm and cleaned as the following step. First, FTO glasses were cleaned with a detergent before being sonicated with a detergent and DI water for 15 min. Second, they were cleaned with DI water and soaked for another 5 minutes, then sonicated with DI water and isopropanol for 15 min each, respectively. Finally, they were purified by UV-ozone for 15 min.

#### 2. Preparation of precursor solution for compact TiO<sub>2</sub> film

TiO<sub>2</sub> precursor for the compact film consists of 0.25 M titanium (IV) isopropoxide and 0.018 M hydrochloric acid. First, 785 μl titanium (IV) isopropoxide and 18 μl hydrochloric acid were dissolved in 5 ml of ethanol separately and then stirred with a magnetic stirrer at 400 rpm and at ambient conditions for 15 min each. Then, the hydrochloric solution was injected into titanium (IV) isopropoxide solution drop by drop with continuous stirring at the same speed for 15 min until the solution became transparent.

#### 3. Preparation of precursor solution for mesoporous TiO<sub>2</sub> film

To synthesize mesoporous TiO<sub>2</sub> film, 1.34 ml hydrochloric acid was added into continuous stirring 2.56 ml titanium (IV) isopropoxide at ambient conditions. Along with the preparation of the surfactant solution, 0.65 g of Pluronic P123 and 11.40 ml of ethanol were stirred until the solution was dissolved. Finally, the surfactant solution was added into titanium (IV) isopropoxide solution and left continuously stirring for 30 min.

#### 4. Film coating

The photoanode material contains TiO<sub>2</sub> films that were deposited on FTO glasses via the convective deposition technique. First, the deposition blade was set at 0.5 mm above the glass substrate before the precursor was injected between the tip of the blade and substrate surface. Then, the substrate was moved at a speed of 0.9 cm/s, while the solution was being pulled in the opposite direction to coat on the substrate. The excess solution was absorbed using delicate task wiper. Second, the substrate which was covered by a thin layer of solution was heated on a hot plate at 70°C for 15 min. The procedure was repeated 3 times to obtain thick films for TiO<sub>2</sub> compact film. Finally, the deposited film was annealed in N<sub>2</sub> atmosphere at 500°C for 1 hr to crystalize the TiO<sub>2</sub> structure.

### 3.2.2 Membrane activation

Nafion 117 proton exchange membrane has to be activated before assembly with the reactor via the following procedure. The membrane was soaked in DI water for 1 hr. 3 wt.% hydrogen peroxide was dissolved in DI water and then the membrane was soaked again in the as-prepared hydrogen peroxide solution and DI water, respectively, at 80°C for 1 hr each. The membrane must be transparent after activation.

### 3.2.3 Oxidation of benzyl alcohol via photoelectrochemical reactor

The component of the PEC reactor is shown in **Figure 3.1** and the detail is described below.

1. Frame: Two pieces of aluminum plates at the outside of the reactor were used for assembling each component. The one on the anode side has a slot hole in the middle for light illumination.
2. Gasket: Two rubber sheets were used to prevent the leaking of liquid in the reactor. The gasket on the anode side also has a slot hole for light illumination.
3. Cathode: A copper plate for reduction reaction at the cathode chamber.
4. Chamber: A rubber sheet with a slot hole in the middle for chemical flow. The volume of the chamber is 3.1 ml each.
5. Membrane: Nafion 117 proton exchange membrane, used to separate the cathode and anode chambers and allow protons to transfer from the anode to the cathode.
6. Aluminum foil: A conductor for electron transfer between photoanode and external wire.
7. Photoanode: compact and mesoporous  $\text{TiO}_2$  films on FTO glasses used for oxidation reaction in anode chamber.

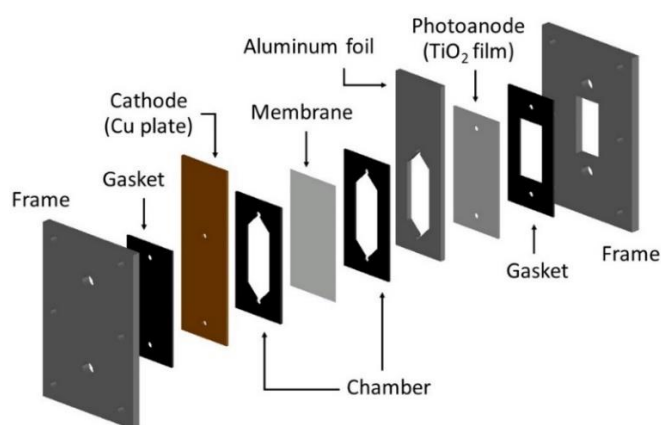


**Figure 3.1** Photoelectrochemical reactor component.

The schematic diagram of the photoelectrochemical system is shown in **Figure 3.2**. The experiment starts with assembling the components of the reactor. There are two different surface morphologies of  $\text{TiO}_2$  including compact film and mesoporous film. The feed composition of the inlet consists of 0.1 M sodium sulfate solution as an electrolyte on both sides and a mixture of 0.02 M benzyl alcohol in the anode side. Two syringe pumps were used to control 4 levels of feed flow rate consisting of 0.05, 0.10, 0.15, and 0.20 ml/min, which were connected to the reactor via polyurethane pipes. The outlet was connected to the collector. A 100 W UV lamp was used as the light source which illuminated the photoanode. Finally, the DC supplier was connected to the photoanode and cathode to apply potential and current density to the system. To evaluate the experiment, percentage conversion and selectivity were calculated via the equations (14) and (15) respectively.

$$\text{Conversion (\%)} = \frac{C_{BA_0} - C_{BA_f}}{C_{BA_0}} \times 100 \quad (14)$$

$$\text{Selectivity (\%)} = \frac{C_{BD}}{C_{BA_0} - C_{BA_f}} \times 100 \quad (15)$$

Where  $C_{BA_0}$  is the initial concentration of benzyl alcohol (mol/l)

$C_{BA_f}$  is the outlet concentration of benzyl alcohol (mol/l)

$C_{BD}$  is the outlet concentration of benzaldehyde (mol/l)

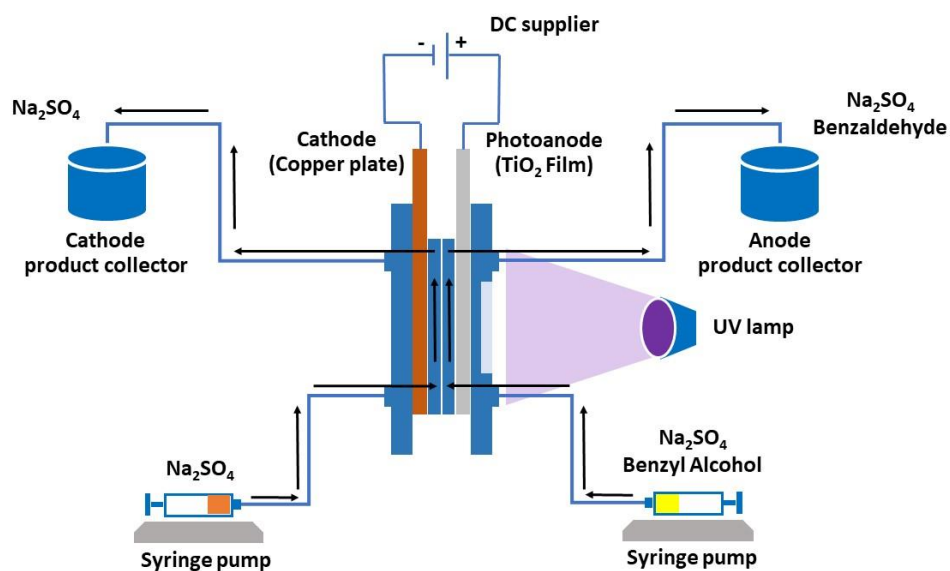


**Figure 3.2** Schematic diagram of the photoelectrochemical system.

### 3.3 Characterization

#### 1) UV-vis spectrophotometer

UV-vis spectrophotometer (Shimadzu UV-2600) was used to determine an absorption of TiO<sub>2</sub> film in the wavelength between 250 to 800 nm. The collected data was also used to calculate band gap energy using Tauc plot.

#### 2) Scanning electron microscope (SEM)

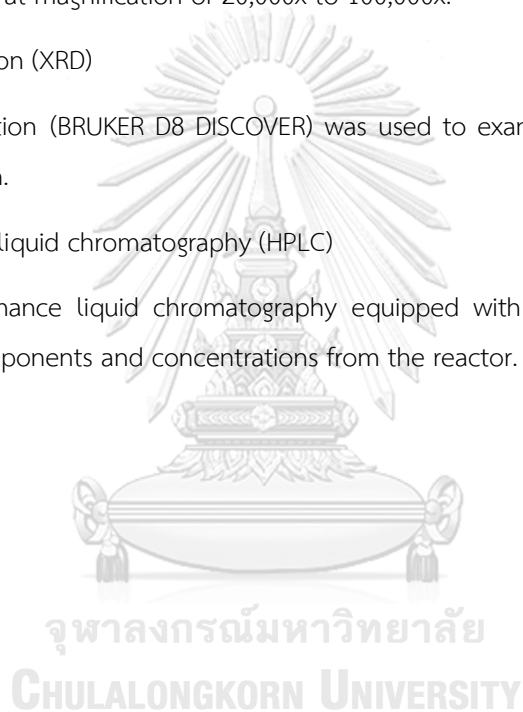
Scanning electron microscope was used to investigate surface morphology and film thickness of TiO<sub>2</sub> film at magnification of 20,000x to 100,000x.

#### 3) X-ray diffraction (XRD)

X-ray diffraction (BRUKER D8 DISCOVER) was used to examine crystallization and phase formation of TiO<sub>2</sub> film.

#### 4) High performance liquid chromatography (HPLC)

High performance liquid chromatography equipped with a C18 column was used to analyze product components and concentrations from the reactor.



## CHAPTER 4

### RESULTS AND DISCUSSION

In this section, the characterization of TiO<sub>2</sub> films including morphology, structure, optical and electrical properties is discussed. The successfully fabricated compact and mesoporous TiO<sub>2</sub> films were used as photoanodes in the photoelectrochemical oxidation of benzyl alcohol. The percentage conversion of benzyl alcohol and the percentage selectivity of benzaldehyde were determined, and the mechanism of the reaction was proposed in this work.

#### 4.1 Morphology and structure of compact and mesoporous TiO<sub>2</sub> films

##### 4.1.1 Morphology characterization

A morphology and film thickness of TiO<sub>2</sub> films prepared by sol-gel method and coated via convective deposition on the FTO glass substrate was examined using Field Emission Scanning Electron Microscope (FE-SEM).

##### 1) TiO<sub>2</sub> mesoporous film

According to **figure 4.1a**, the rough uniform surface of the mesoporous film is successfully synthesized. The cross-section in **figure 4.1b** indicates two visible layers, which are a smooth layer of TiO<sub>2</sub> on the top surface and a rough surface layer of FTO at the bottom, resulting in varying thicknesses of TiO<sub>2</sub> ranges from 375 nm to 520 nm with the average range of 454 nm. The top layer of TiO<sub>2</sub> presents a fluffy layer indicating a mesoporous structure due to the addition of Pluronic P123, the primary role of a structure-directing agent, creates the mesoporous structure in the TiO<sub>2</sub> structure. The mechanism of the process starts with the titanium precursor undergoing hydrolysis and condensation in the dissolved P123 solvent. The P123 assembled with the solution to form micelles contain an opposite direction of hydrophobic and hydrophilic in the same molecule. Then, the hydrophobic side reacts with the forming TiO<sub>2</sub> and prevents them from gathering together. Finally, the remaining P123 is eliminated via calcination leaving the mesoporous structure to remain in the product.[51]

##### 2) TiO<sub>2</sub> compact film

The top view of TiO<sub>2</sub> film on the FTO glass substrate is shown in **figure 4.1c**. The film synthesized with a compact and uniform layer free of cracks and impurities. Two layers of



TiO<sub>2</sub> and rough FTO are also visible in the cross-sectional image (**Figure 4.1d**), resulting in varying thicknesses of TiO<sub>2</sub> from 140 to 290 nm. The average film thickness is determined to be 218 nm. However, the compact layer seemed similar to the mesoporous, indicating a possibility of porous forming inside the material either macropore or mesopore. So, the BET N<sub>2</sub> adsorption is necessary to determine the porosity of compact film as well.

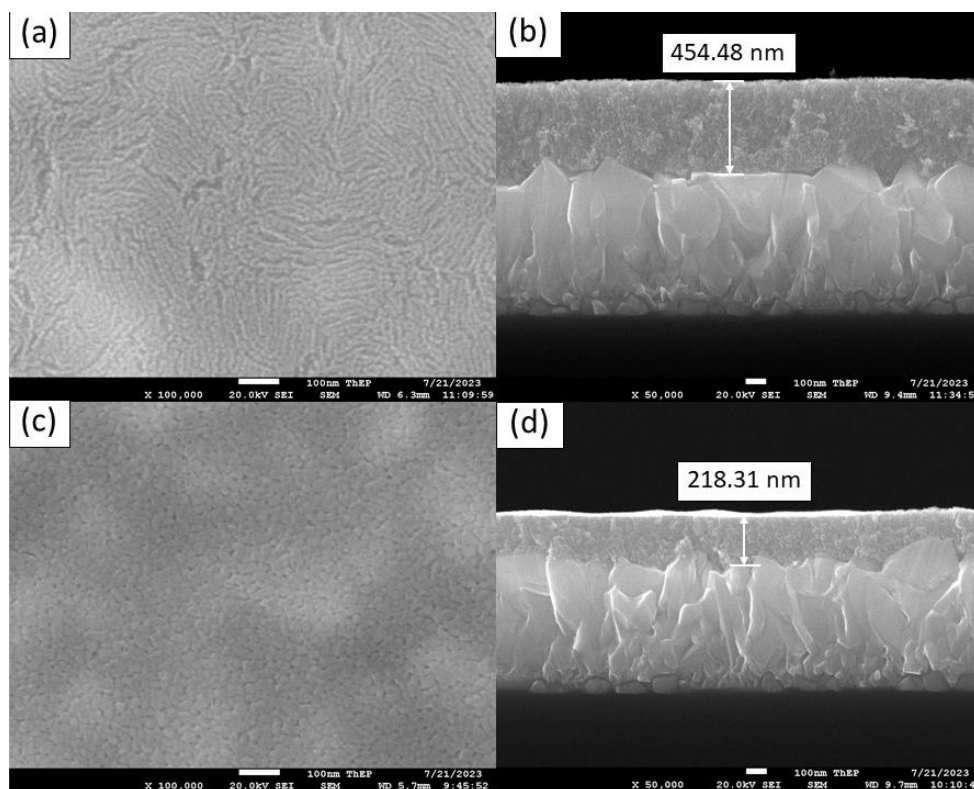


**Figure 4.1** SEM micrographs showing (a) surface morphology of mesoporous TiO<sub>2</sub> film (b) cross-sectional image of mesoporous TiO<sub>2</sub> film, (c) surface morphology of compact TiO<sub>2</sub> film, and (d) cross-sectional image of compact TiO<sub>2</sub> film.

#### 4.1.2 Structure characterization

The crystallinity of TiO<sub>2</sub> films were characterized using X-ray diffraction (XRD), as shown in **figure 4.2**. The crystalline structure of TiO<sub>2</sub> compact film was detected with the peaks of  $2\theta$  at 25.29°, 38.70°, and 47.97° referring to the planes (101), (004), and (200), respectively, which demonstrated the anatase phase of TiO<sub>2</sub>. While the other peaks at 26.49°, 33.69°, 37.71°, 51.53°, and 54.56° are referred to the FTO layer. In the case of TiO<sub>2</sub> mesoporous film, only the peak at 25.3° which corresponds to the (101) plane can be detected. This is due to the lower calcine temperature at 450°C, while the compact film was calcined at 500°C. The lower and broader peak at 25.3° of TiO<sub>2</sub> mesoporous film refers to a high content of amorphous TiO<sub>2</sub> that can

decrease with the growth of the anatase phase due to the increase in temperature. In general, the anatase phase usually requires a temperature of at least 300°C to convert the amorphous TiO<sub>2</sub> into the anatase phase and avoid surpassing 600°C to prevent the formation of a rutile phase. Although increasing calcine temperature can enhance the crystallinity of the anatase phase, the synthesis of mesoporous material still cannot use the temperature as high due to the mesoporous structure could collapse with an increase in temperature. [51] Besides, the full-width half maximum of the anatase phase at 2θ is 25.3° was used to determine the crystallite size of anatase TiO<sub>2</sub> and the result shows the size of 8.48 and 16.78 nm. and the relative intensity found to be 5.8 and 14.3% for mesoporous and compact respectively which indicated the content of TiO<sub>2</sub> anatase phase in compact film is higher than mesoporous film.

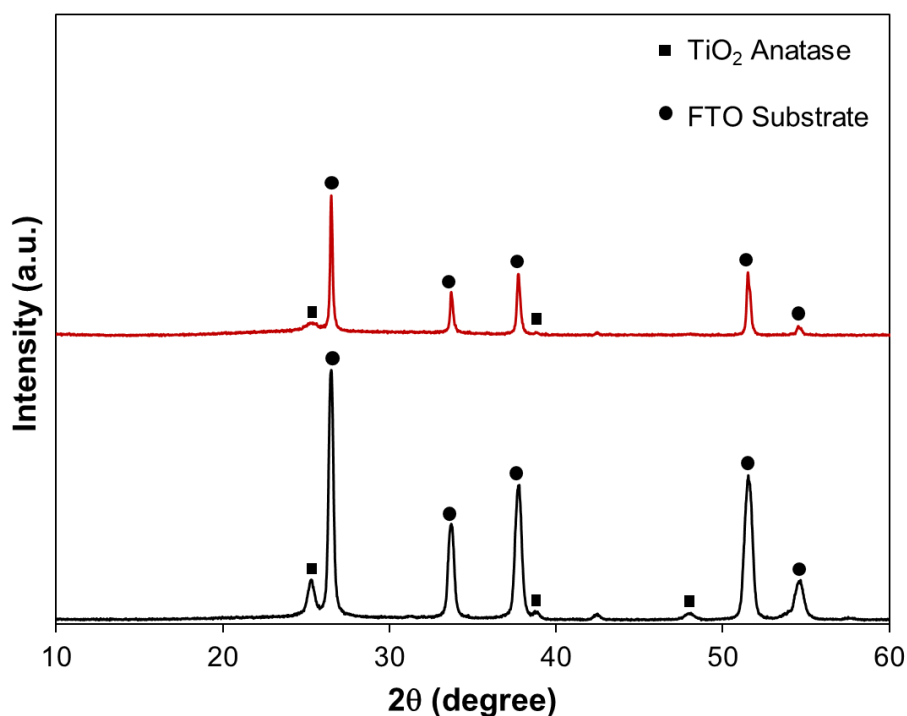


**Figure 4.2** XRD patterns of compact (black) and mesoporous (red) TiO<sub>2</sub> films deposited on FTO glasses.

#### 4.1.3 Surface area analysis

The synthesized mesoporous TiO<sub>2</sub> film was scratched off from the substrate to collect as mesoporous TiO<sub>2</sub> powder before being carried on to characterize the specific surface area using N<sub>2</sub> adsorption. The adsorption isotherm was analyzed and shown in **figure 4.3**. Firstly, the increase of the relative pressure leads the N<sub>2</sub> molecules to adsorb on the available active site in

the form of a monolayer which is the slow increase of quantity adsorbed in the first period (relative pressure below 0.6). Then, the continuous increase of relative pressure affects the process of starting the multilayer adsorption in the pore before capillary condensation occurs at below saturated pressure due to the increase of van-der-Waals force of molecule in a limiting space, resulting in a rapid increase of quantity adsorbed (relative pressure over 0.7). Finally, the decreasing relative pressure appears as the desorption of  $N_2$  molecule at lower relative pressure than adsorption because of the strong interaction between molecules in the pore, more energy is required to remove which appears as a “hysteresis loop”.[52] These phenomena of adsorption and desorption can be categorized as type IV isotherm due to the presence of a hysteresis loop that relates to the behavior of mesoporous material which has pores size between 2 – 50 nm. The pores shape can be presumed as cylindrical judging from the hysteresis loop appearance. The pore size distribution of mesoporous  $TiO_2$  film, as shown in **figure 4.4**, is mostly in the range of 5 – 30 nm with a few pores over 40 nm in size. An average pore size, specific surface area, and pore volume are reported in **table 3**. The surface area of the synthesized mesoporous  $TiO_2$  film appears to be within a reasonable range compared to previous research, but still lower than those of some work that used lower calcining temperatures. The large pore size and pore volume enhances the reactant and product diffusion but it also makes the material stability decrease.

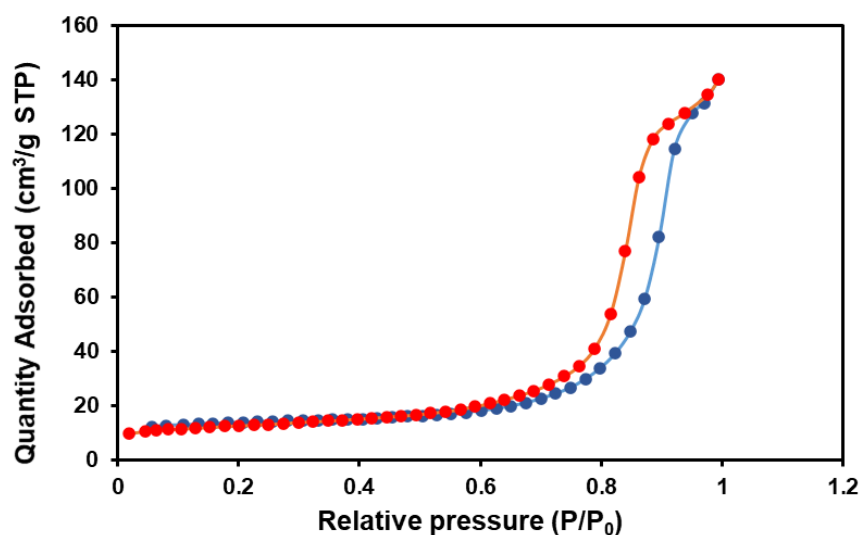


Figure 4.3  $N_2$  adsorption and desorption isotherm of mesoporous  $TiO_2$  film.

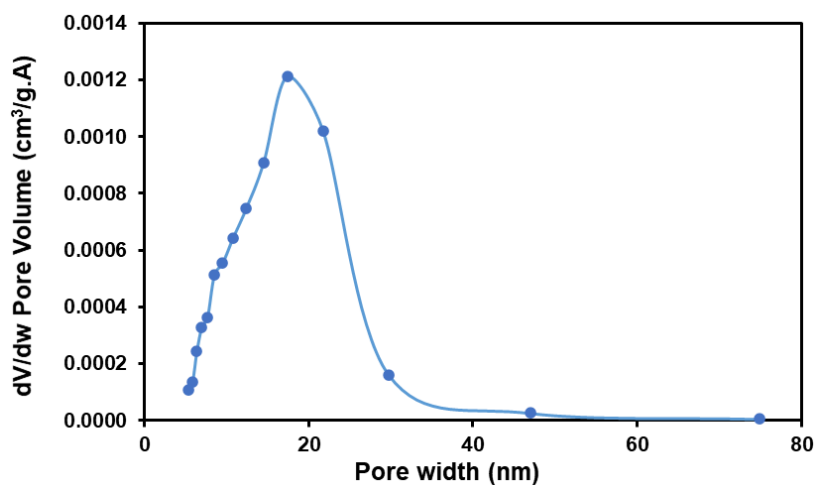


Figure 4.4 Pore size distribution of mesoporous TiO<sub>2</sub> film.

Table 3 Specific surface area of mesoporous TiO<sub>2</sub> film

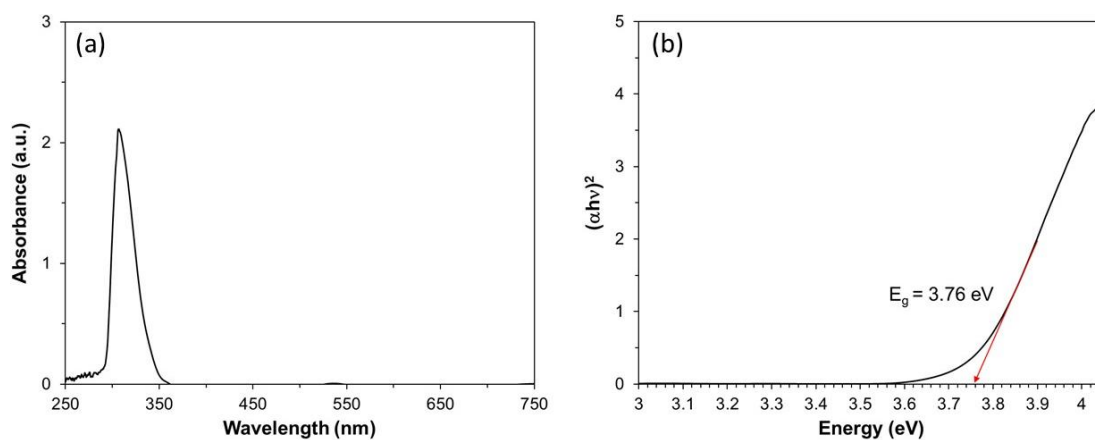
Research	Structure-Directing Agent	Calcining temperature (°C)	Specific surface area (m <sup>2</sup> /g)	Pore size (nm)	Pore volume (cm <sup>3</sup> /g)	Ref
This work	Pluronic P123	450	44.02	17.43	0.198	-
A. Granados et al.	Polyvinylpyrrolidone	550	40.79	12.70	0.079	[53]
M. Zakaria et al.	Pluronic P123	400	62.00	5.30	0.098	[51]
M. Zakaria et al.	Pluronic P123	550	23.00	8.70	0.061	[51]

## 4.2 Optical and electrical properties of compact and mesoporous TiO<sub>2</sub> films

### 4.2.1 Optical properties

A UV-Vis spectrophotometer (Figure 4.5a, c) was used to analyze the optical properties and find the material's absorption wavelength. Both mesoporous and compact TiO<sub>2</sub> films exhibit the characteristics of UV light excitation by absorbing light in the 290–350 nm range, peaking at 305 nm, which is within the UV spectrum. The optical band gap energy ( $E_g$ ) of the TiO<sub>2</sub> film, which was identified as an indirect band gap material, was also examined using the Tauc plot and discovered to be 3.7 eV (Figure 4.5b, d). The large band gaps also prove that TiO<sub>2</sub> prefers high-energy light sources, like UV light, to excite and generate charge carriers, making it appropriate for reactions that require high energy to suppress their activation energy.

### Compact film



### Mesoporous film

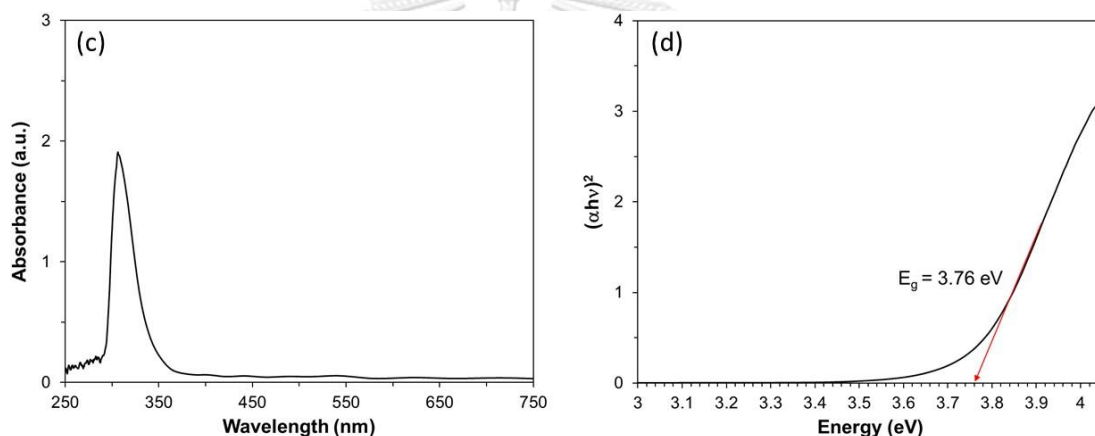


**Figure 4.5** Optical analysis of (a, c) UV-Vis absorbance, and (b, d) optical band gap energy of compact and mesoporous  $\text{TiO}_2$  films.

#### 4.2.2 Electrical properties

The electrochemical performance of compact and mesoporous  $\text{TiO}_2$  films used as photoanodes was analyzed using three electrode systems in an electrochemical H-cell. The fabricated  $\text{TiO}_2$  film was used as the working electrode, platinum mesh as a counter electrode, and  $\text{Ag}/\text{AgCl}$  in 0.1 M  $\text{KCl}$  as a reference electrode. The electrode was submerged in 0.1 M  $\text{Na}_2\text{SO}_4$  electrolyte containing 0.2 M benzyl alcohol. **Figure 4.6** shows the cyclic voltammetry at 500 mV/s with a potential window between -4 to 4 V. The result shows the current of mesoporous film at 4 V is 0.0123 mA which is higher than 0.0098 mA of the compact film, indicating a lower resistance and better electron transfer than the compact film. It is possible that the light utilizes a longer time inside the mesoporous material due to the more porosity and thickness of the film,

and results in a higher photo-generate charge. In terms of stability, the compact film seems to have more durability than the mesoporous film according to the invariable of the graph after 10 cycles while the mesoporous film slightly decreased.

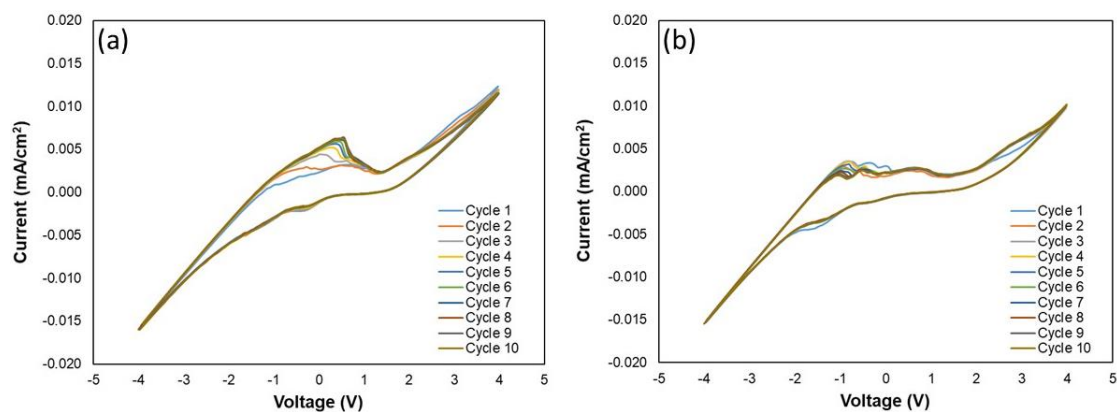


Figure 4.6 Cyclic voltammety of (a) Mesoporous  $\text{TiO}_2$  film and (b) Compact  $\text{TiO}_2$  film.

### 4.3 Photoelectrochemical oxidation of benzyl alcohol

#### 4.3.1 Standard calibration

To characterize what was obtained from the photoelectrochemical oxidation, HPLC equipped with a C18 column was used to determine the compositions of the product. The test conditions are as follows: UV detector 254 nm, methanol to water ratio at 48:52 with the flow rate at 0.8 mL/min. The standard test represents benzyl alcohol and benzaldehyde peaks at the retention time of 5.7 and 7.5 min, respectively, as shown in **figure 4.7**. The calibration curve was calculated by varying concentrations of the samples containing 0.005, 0.01, 0.015, 0.02, 0.025 mol/min for benzyl alcohol and 0.001, 0.002, 0.003, 0.004, 0.005 mol/min for benzaldehyde. The relationship between concentration and area of the chromatogram is shown in **table 4**.

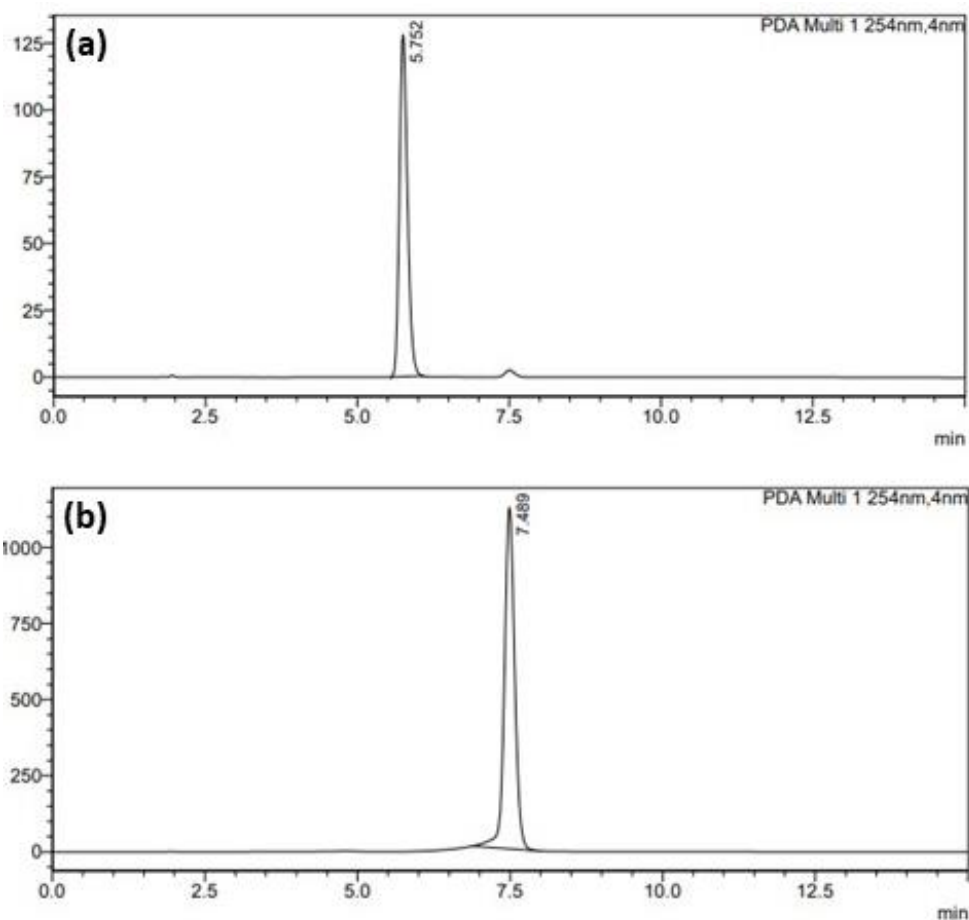


Figure 4.7 HPLC Chromatograms of the standard of (a) benzyl alcohol and (b) benzaldehyde.

Table 4 The relationship between concentration and area of chromatogram

Chemical	Relationship	R <sup>2</sup>
Benzyl alcohol	$Y = (5.922 \times 10^7) X + (6.653 \times 10^3)$	99.99%
Benzaldehyde	$Y = (2.656 \times 10^9) X + (2.335 \times 10^5)$	99.84%

Where X is the concentration of benzyl alcohol or benzaldehyde (M)

Y is the area of the peak (mAU).

#### 4.3.2 Effect of electrolyte flow rate on benzyl alcohol conversion

In this experiment, the reactants were fed through the 1 cm<sup>3</sup> chamber with rectangular-shaped cross-sectional to undergo oxidation reaction. The different film morphology of mesoporous and compact film used as photoanode with a varying solution flow rate of 0.05,

0.10, 0.15, and 0.20 mL/min, which indicated the Reynold number of 1.64, 3.29, 4.92, and 6.55 respectively. It shows a laminar flow of fluid inside the reactor chamber, indicating that different surface roughness of mesoporous and compact film has no effect on flow characteristics due to the independence between friction factor and relative roughness. **Figure 4.8** shows the percentage conversion of benzyl alcohol at different flow rates using mesoporous and compact TiO<sub>2</sub> films as photoanodes. At all flow rates, the reaction in a continuous-flow reactor can attain a steady state within 15 minutes, because the graphs appear to reach a plateau after that. However, due to the limited equipment and small-scale setup, a collection of samples from the reaction before 15 min could not be carried out. The relationship between flow rate and conversion obtained from both compact and mesoporous TiO<sub>2</sub> films demonstrates that the conversion of benzyl alcohol increases as the solution flow rate decreases. This is because a longer residence time can be carried out at lower flow rates. Letting the reactant interact with the catalytic material and undergo the photoelectrochemical process longer results in an increasing conversion rate. Moreover, it can be observed from the graph that at the low flow rates of 0.05 and 0.1 mL/min, the different morphology has no significant impact on benzyl alcohol conversion (**figure 4.9a**). While at the high flow rates of 0.15 and 0.1 mL/min, the mesoporous film can produce a higher conversion rate (**figure 4.9b**), which shows the effect of different morphology between compact and mesoporous film. The XRD result detected the higher crystallinity of anatase phase TiO<sub>2</sub> in compact film, while the mesoporous film gains an advantage of higher surface area. Here, the result can conclude that surface area has more impact on the benzyl alcohol conversion than the content of the anatase phase.

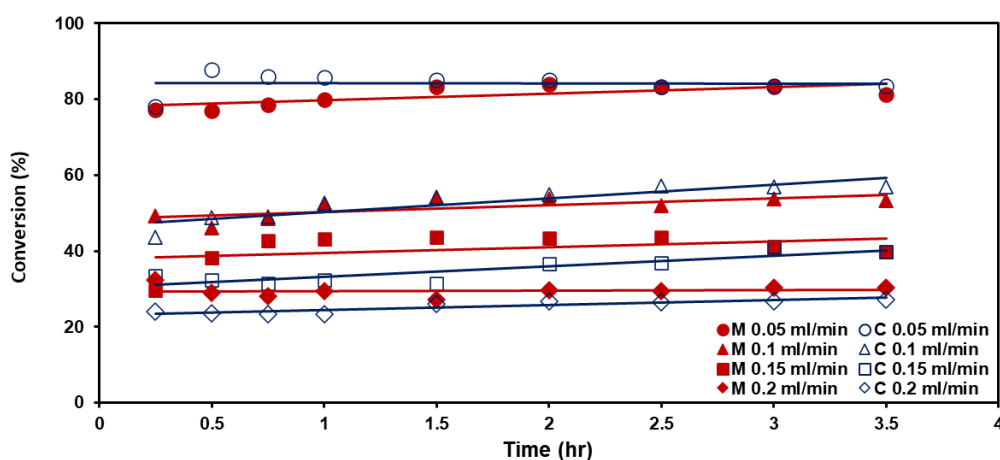


**Figure 4.8** Effect of electrolyte flow rate on conversion of benzyl alcohol.



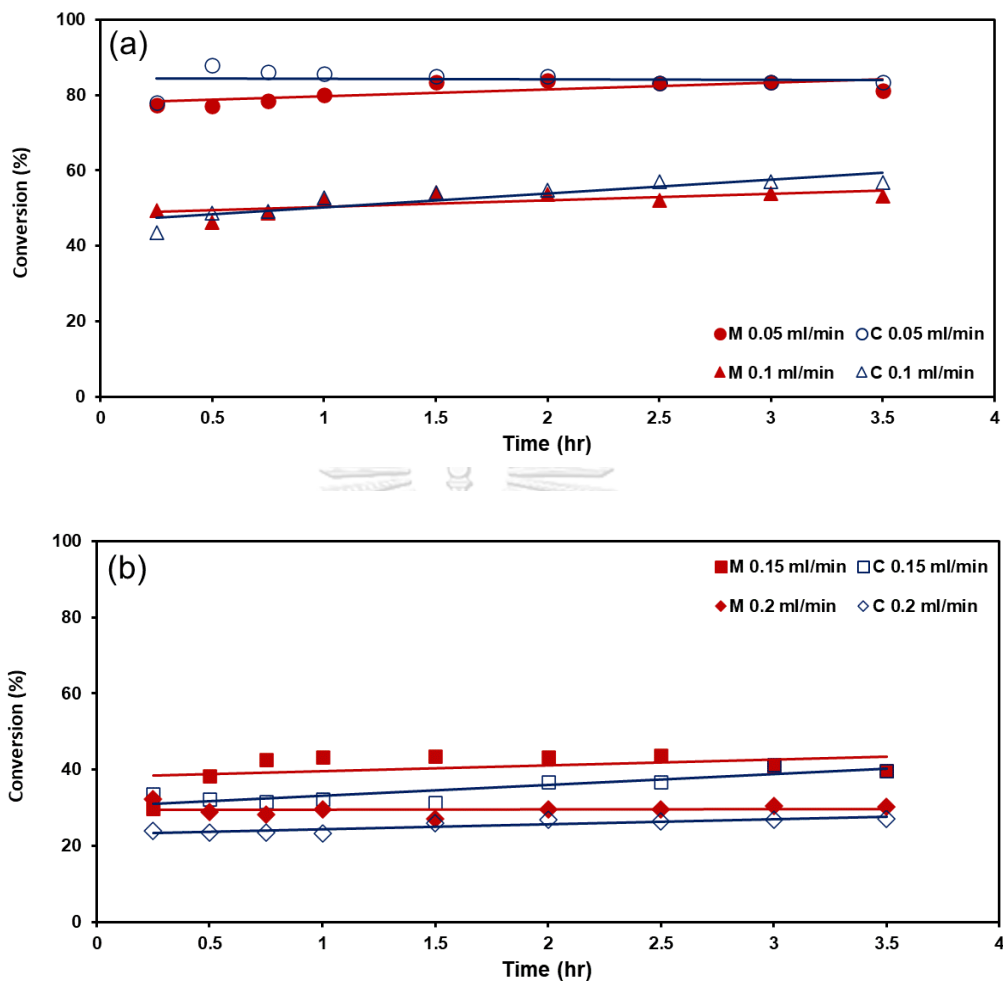


**Figure 4.9** Comparison of conversion of benzyl alcohol using mesoporous and compact TiO<sub>2</sub> films as photoanode at flow rates of (a) 0.05, 0.1 ml/min and (b) 0.15, 0.2 ml/min.

#### 4.3.3 Effect of electrolyte flow rate on benzaldehyde selectivity

**Table 5** indicates that the benzaldehyde selectivity improved with the increase of solution flow rate until the flow rate of 0.15 ml/min. In the case of mesoporous film, the selectivity appears to be steady even with a further increase in solution flow rate. The highest selectivity of 50.59% can be obtained from 0.15 ml/min. On the other hand, the selectivity of the compact film decreases after 0.15 ml/min, therefore the maximum selectivity of 45.28% can be achieved at this flow rate. This can also be explained by the effect of residence time. Increasing residence time as a result of decreasing flow rate, can enhance the benzyl alcohol conversion rate by extending the reaction time. However, the side reactions or the overoxidation of

benzaldehyde can also occur and overcome the main reaction, therefore reducing the amount of benzaldehyde produced.

**Table 5** Benzaldehyde percentage selectivity using mesoporous and compact film after 1.5 hr

Photoanode	Flow rate (ml/min)	Benzaldehyde selectivity (%)
Mesoporous film	0.05	13.97
	0.10	40.80
	0.15	50.59
	0.20	50.13
Compact film	0.05	10.02
	0.10	43.11
	0.15	45.28
	0.20	34.41

#### 4.3.4 The proposed reaction pathways of benzyl alcohol

The benzyl alcohol reaction pathways were investigated to find the possible byproducts that could be obtained from photoelectrochemical reactions. Although benzyl alcohol is an aromatic alcohol with a moderate level of reactivity, the presence of a hydroxyl group influences to many possible reactions. **Figure 4.10** shows the possible reaction pathways of benzyl alcohol which contain benzaldehyde as the main target oxidation. Since the experiment is set in the ambient conditions which environment surrounded by oxygen, the benzaldehyde can be oxidized by existing oxygen and undergo overoxidation to become benzoic acid. Benzoic acid can further react with benzyl alcohol to undergo esterification and form benzyl benzoate. Moreover, benzyl alcohol has the potential to undergo side reactions including hydrogenolysis to toluene and decarbonylating to benzene. Among these byproducts, it seems benzoic acid which is on the same oxidation pathways as benzaldehyde and benzyl benzoate used benzyl alcohol, benzaldehyde, and benzoic acid as reactants are most possible. Benzoic acid and benzyl benzoate are valuable components in pharmaceuticals, foods, and cosmetics. The price varies depending on the purity up to 150 USD/L for 99% purity. On the other hand, benzene is an important ingredient in chemical production such as polymer and an organic solvent, while toluene can be used for painting, adhesive, and fuel industries, their value is also relatively high. In summary, the byproducts from photoelectrochemical oxidation of benzyl alcohol are required in many industries which demonstrate the high potential in terms of economics.

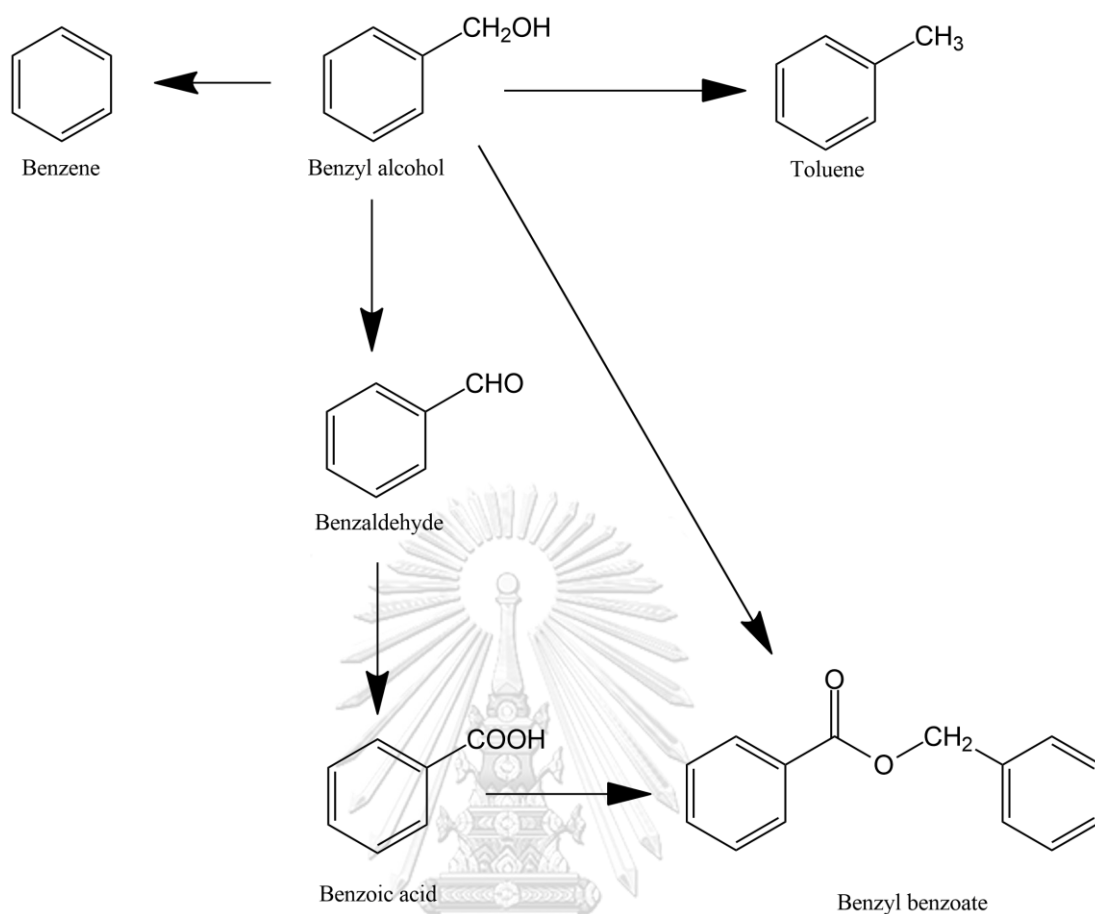


**Figure 4.10** The reaction pathways of benzyl alcohol.

#### 4.3.5 Effect of other factors on percentage conversion and selectivity

In this section, various other factors were examined to evaluate the performance of the continuous-flow photoelectrochemical reactor. First, the effect of different light sources was explored by using a UV lamp, natural light, and dark environments. The photocatalytic activity was also evaluated using a UV lamp without any electrical source. Second, the effect of continuous flow by comparing to the batch-type reactor using an “electrochemical H-cell”. **Figure 4.11a, b** illustrates the percentage conversion and selectivity using the compact  $\text{TiO}_2$  film as photoanode at a flow rate of 0.1 mL/min under UV-light, natural light, and dark conditions. The conversion still reached a steady state before 15 min when the light source was changed. However, the result indicated a decrease in overall conversion when the source was changed from UV light. In terms of selectivity, a similar trend is observed when comparing to the previous result, in which the selectivity increases with time, then becomes steady after 1.5 hr. The other environments except UV light also have a significant decrease. The reason behind this is a decrease in charges generated from photo-excitation in  $\text{TiO}_2$  photoanode. The anatase phase of

TiO<sub>2</sub> has a large band gap of 3.2 eV, therefore requiring a light with high energy to promote the electron from the valance band to the conduction band. In this case, the appropriate light energy source used for exciting the electron in the valance band is UV light, so the decrease in conversion is observed in a natural and dark condition. Unfortunately, the photocatalysis reaction cannot detect any change in the composition of the reactant because a longer retention time is required. Here, the experiment shows the main role of both light and the electricity to promote the oxidation reaction. In batch type reactor, the conversion of benzyl alcohol steadily increases even after 6 hr, and it does not seem to even reach a plateau. After 6 hr of reaction, only 16.29% of benzyl alcohol is converted which is lower than that obtained from the fastest flow rate of 0.2 ml/min in a continuous flow reactor. The conversion and selectivity of different conditions are summarized and compared to the highest value, as shown in **table 6**.

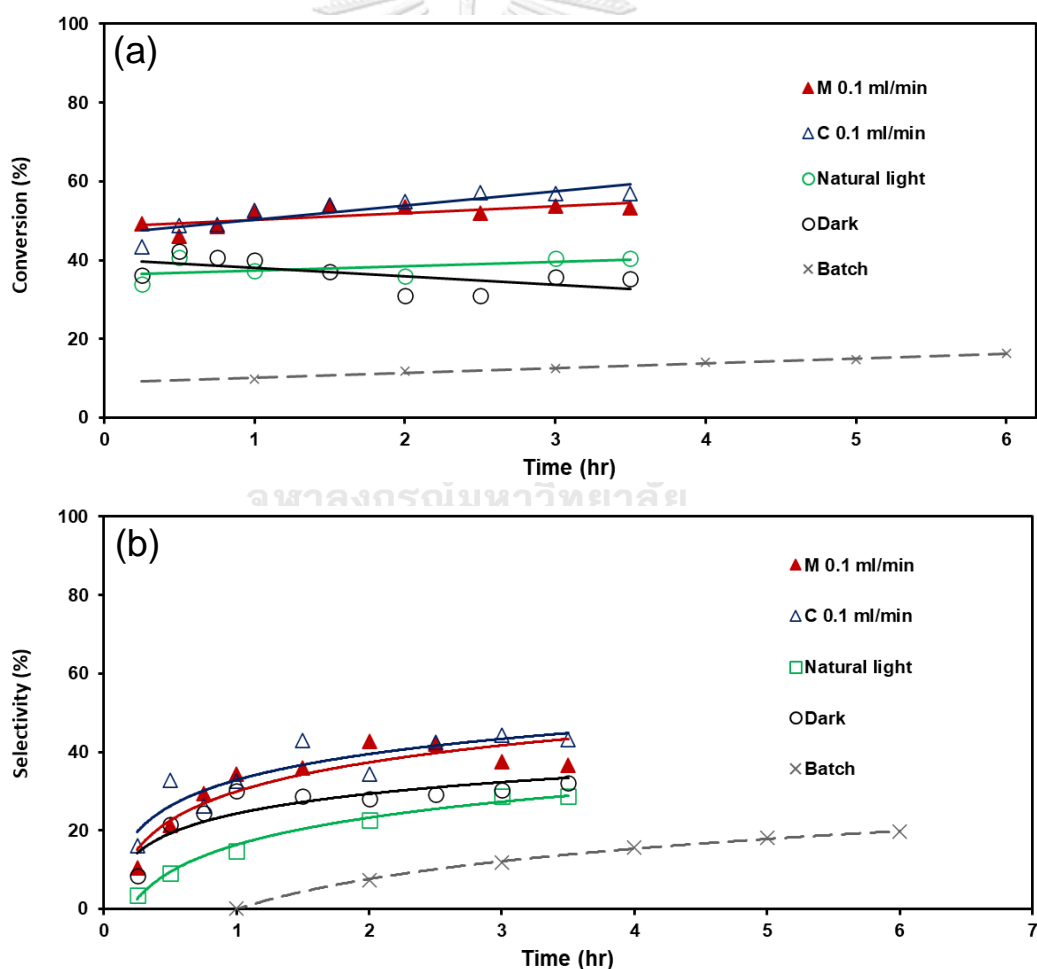


**Figure 4.11** Photoelectrochemical effects from different factors on (a) benzyl alcohol conversion and (b) benzaldehyde selectivity.

**Table 6** Performance comparison of PEC oxidation of benzyl alcohol under different conditions

Type	Flow rate/ reaction time	Light	Conversion (%)	Efficiency (%)	Selectivity (%)	Efficiency (%)
Continuous flow	0.05 ml/min	UV	84	<b>100</b>	10	23
	0.1 ml/min	UV	56	67	43	<b>100</b>
	0.1 ml/min	Natural	39	41	29	67
	0.1 ml/min	Dark	34	40	32	74
Batch	6 hr	UV	16	19	25	58

**Table 7** demonstrates a comparison of conversion and selectivity in photoelectrochemical oxidation of benzyl alcohol with the recent literatures. The result shows an outclass of conversion and/or selectivity in many cases even a slight value, but it can perform more than 4 hr faster. Herein, the remarkable performance of the continuous-flow reactor over the batch-type reactor is confirmed. However, these results exhibit 2 important aspects that can improve the system efficiency. First, the presence of oxygen in the oxidation reaction is of important. The continuous-flow photoelectrochemical reactor needs to be customized in terms of gas support, not only for the flow of oxygen gas but also hydrogen gas collected from the reduction reaction at the cathode side. The other key factor is the photoanode. The selectivity is mainly dependent on the suitable catalyst used in the reaction. Although  $\text{TiO}_2$  has high physical and chemical properties in the photocatalyst field, it still needs to be improved for the specific reaction.

**Table 7** Performance comparison of PEC oxidation of benzyl alcohol to recent literature

Type	Electrode	Condition	Flow rate /reaction time	Conversion (%)	Selectivity (%)	Ref.
Continuous flow	Anode: $\text{TiO}_2$ Cathode: Cu	Anaerobic	0.1 ml/min after 1.5 hr	56	43	This work
Batch	Anode: $\text{TiO}_2$ Cathode: Cu	Anaerobic	6 hr	16	20	This work
Batch	Anode: $\text{Bi}_2\text{MoO}_6@ \text{TiO}_2$ Cathode: C/ $\text{Cu}_2\text{O}$	Aerobic	8 hr	67	99	[39]

Type	Electrode	Condition	Flow rate /reaction time	Conversion (%)	Selectivity (%)	Ref.
Batch	Anode: $\text{Bi}_2\text{MoO}_6@\text{TiO}_2$ Cathode: C/ $\text{Cu}_2\text{O}$	Anaerobic	8 hr	48	46	[39]
Batch	Anode: $\text{TiO}_2$ NTA Cathode: C/ $\text{Cu}_2\text{O}$	Aerobic	8 hr	69	58	[39]
Batch	Anode: $\text{TiO}_2$ NTA Cathode: C/ $\text{Cu}_2\text{O}$	Anaerobic	8 hr	51	37	[39]



## CHAPTER 5

### CONCLUSION AND RECOMMENDATION

#### 5.1 Conclusion

The continuous flow photoelectrochemical reactor was fabricated successfully with a performance that overcame traditional batch-type reactors. The conversion can reach a steady state within 15 min, while batch-type reactors require longer than 6 hr. The most impactful part is the narrow chambers in a continuous flow reactor, which offer a shorter path length for charge transport and ion species to diffuse onto the electrode surfaces. The mixing performance due to concentration gradient was also improved.

The decrease in the electrolyte flow rate shows an improvement in the conversion of benzyl alcohol, while the benzaldehyde selectivity decreases. Both variables are directly affected by the retention time. The longer retention time can produce a high conversion rate, but the extension of retention time also makes the solution in the reactor undergo overoxidation or side reaction, resulting in a decrease in the selectivity of the target product. At a low electrolyte flow rate, the effect of different morphology is insignificant. While mesoporous TiO<sub>2</sub> film dominates at faster flow rates, indicating the surface area of the material has more impact in the photoelectrochemical process than the existing of anatase phase. After 1.5 hr, the optimal conditions obtained from the compact TiO<sub>2</sub> film is a flow rate of 0.1 ml/min with an average benzaldehyde yield of 24.15%. For mesoporous TiO<sub>2</sub> film, the average benzaldehyde yield of 21.32% was achieved at a flow rate of 0.15 ml/min. Even though the percentage yield obtained from the mesoporous film is lower than that of the compact film, the condition using the mesoporous film was carried out with a flow rate 50% faster, indicating that using mesoporous film has a faster production rate of benzaldehyde. Lastly, the experiment in dark condition produced less conversion and selectivity, confirming that both light and electricity promoted the reaction, which is the highlight of the photoelectrochemical process.

#### 5.2 Recommendation

##### 5.2.1 Effect of current and voltage

Study on the effect of current and voltage that affect the benzyl alcohol conversion and benzaldehyde selectivity.

### 5.2.2 Effect of reactor volume

Study the relationship between electrolyte flow rate and reactor volume to improve the benzaldehyde production rate to determine the optimal condition.

### 5.2.3 Support for gas system

Another main product from photoelectrochemical oxidation of benzyl alcohol is hydrogen gas at the cathode side. The continuous-flow reactor needs a development to support gas in the system.







จุฬาลงกรณ์มหาวิทยาลัย  
**CHULALONGKORN UNIVERSITY**

## REFERENCES

1. Kampouri, S. and K.C. Stylianou, *Dual-Functional Photocatalysis for Simultaneous Hydrogen Production and Oxidation of Organic Substances*. ACS Catalysis, 2019. **9**(5): p. 4247-4270.
2. Tayyab, M., et al., *Simultaneous hydrogen production with the selective oxidation of benzyl alcohol to benzaldehyde by a noble-metal-free photocatalyst VC/CdS nanowires*. Chinese Journal of Catalysis, 2022. **43**(4): p. 1165-1175.
3. Joy, J., J. Mathew, and S.C. George, *Nanomaterials for photoelectrochemical water splitting – review*. International Journal of Hydrogen Energy, 2018. **43**(10): p. 4804-4817.
4. Lee, S.G., et al., *Selective photocatalytic conversion of benzyl alcohol to benzaldehyde or deoxybenzoin over ion-exchanged CdS*. Applied Catalysis B: Environmental, 2022. **304**.
5. Wu, Z., et al., *Highly selective aerobic oxidation of biomass alcohol to benzaldehyde by an in situ doped Au/TiO<sub>2</sub> nanotube photonic crystal photoanode for simultaneous hydrogen production promotion*. Journal of Materials Chemistry A, 2017. **5**(24): p. 12407-12415.
6. Toe, C.Y., et al., *Advancing photoreforming of organics: highlights on photocatalyst and system designs for selective oxidation reactions*. Energy & Environmental Science, 2021. **14**(3): p. 1140-1175.
7. Justinus A.B. Satrio, L.K.D., *Production of benzaldehyde a case study in a possible industrial*. Chemical Engineering Journal, 2001. **82**: p. 43-56.
8. Pugh, S., et al., *Engineering Escherichia coli for renewable benzyl alcohol production*. Metab Eng Commun, 2015. **2**: p. 39-45.
9. Rodrigues, C.J.C. and C. de Carvalho, *Process Development for Benzyl Alcohol Production by Whole-Cell Biocatalysis in Stirred and Packed Bed Reactors*. Microorganisms, 2022. **10**(5).
10. Scognamiglio, J., et al., *Fragrance material review on benzyl alcohol*. Food

Chem Toxicol, 2012. **50 Suppl 2**: p. S140-60.

11. *Kirk-Othmer Encyclopedia of Chemical Technology Vol 4.*
12. Insights, B.R. *Benzaldehyde Market Size, Share, Growth, and Industry Analysis by Type (FCC Grade and Technical Grade) By Application (Spices, Pharmaceuticals, Agricultural, and Dye) Regional Forecast To 2028.* 2022; Available from: <https://www.businessresearchinsights.com/market-reports/benzaldehyde-market-101517#:~:text=The%20global%20Benzaldehyde%20market%20size,4.4%25%20during%20the%20forecast%20period.>
13. KGaA, M. *Benzaldehyde.* Available from: [https://www.sigmaaldrich.com/TH/en/search/benzaldehyde?focus=products&page=1&perpage=30&sort=relevance&term=benzaldehyde&type=product\\_name.](https://www.sigmaaldrich.com/TH/en/search/benzaldehyde?focus=products&page=1&perpage=30&sort=relevance&term=benzaldehyde&type=product_name.)
14. Laasri, L. and M. El Makhfi, *Ecofriendly oxidation of benzyl alcohol to benzaldehyde using Zr-Ni/Natural phosphate as an efficient and recyclable heterogeneous catalyst.* Materials Today: Proceedings, 2020. **31**: p. S156-S161.
15. Pugh, L.A., *Understanding catalytic processes used in the fragrance industry,* in *Philosophy.* 2011, University of Glasgow.
16. Idrees, F., et al., *Photoelectrochemical properties for metal oxide-carbon hybrid materials,* in *Metal Oxide-Carbon Hybrid Materials.* 2022. p. 75-102.
17. Xu, X., Q. Zhou, and D. Yu, *The future of hydrogen energy: Bio-hydrogen production technology.* International Journal of Hydrogen Energy, 2022. **47**(79): p. 33677-33698.
18. <Hydrogen percentage.pdf>.
19. Kayfeci, M., A. Keçebaş, and M. Bayat, *Hydrogen production,* in *Solar Hydrogen Production.* 2019. p. 45-83.
20. Megia, P.J., et al., *Hydrogen Production Technologies: From Fossil Fuels toward Renewable Sources. A Mini Review.* Energy & Fuels, 2021. **35**(20): p. 16403-16415.
21. Decker, F. and S. Cattarin, *PHOTOELECTROCHEMICAL CELLS OVERVIEW.* 2009.
22. Li, X., Z. Wang, and L. Wang, *Metal-Organic Framework-Based Materials for*

- Solar Water Splitting*. *Small Science*, 2021. **1**(5).
23. <Thorphan\_Thesis (1).pdf>.
  24. Kalanur, S.S., L.T. Duy, and H. Seo, *Recent Progress in Photoelectrochemical Water Splitting Activity of WO<sub>3</sub> Photoanodes*. *Topics in Catalysis*, 2018. **61**(9-11): p. 1043-1076.
  25. Wang, F. and S.S. Stahl, *Electrochemical Oxidation of Organic Molecules at Lower Overpotential: Accessing Broader Functional Group Compatibility with Electron-Proton Transfer Mediators*. *Acc Chem Res*, 2020. **53**(3): p. 561-574.
  26. Parrino, F., et al., *Properties of titanium dioxide*, in *Titanium Dioxide (TiO<sub>2</sub>) and Its Applications*. 2021. p. 13-66.
  27. Zhang, Q. and C. Li, *High Temperature Stable Anatase Phase Titanium Dioxide Films Synthesized by Mist Chemical Vapor Deposition*. *Nanomaterials (Basel)*, 2020. **10**(5).
  28. Wang, Y.-H., et al., *A Review on the Pathways of the Improved Structural Characteristics and Photocatalytic Performance of Titanium Dioxide (TiO<sub>2</sub>) Thin Films Fabricated by the Magnetron-Sputtering Technique*. *Catalysts*, 2020. **10**(6).
  29. Macwan, D.P., et al., *Thermal plasma synthesis of nanotitania and its characterization*. *Journal of Saudi Chemical Society*, 2014. **18**(3): p. 234-244.
  30. Bellardita, M., S. Yurdakal, and L. Palmisano, *Synthesis and characterization of titanium dioxide and titanium dioxide-based materials*, in *Titanium Dioxide (TiO<sub>2</sub>) and Its Applications*. 2021. p. 87-165.
  31. Yang, G. and S.J. Park, *Conventional and Microwave Hydrothermal Synthesis and Application of Functional Materials: A Review*. *Materials (Basel)*, 2019. **12**(7).
  32. ผลนาค, ฉ., การสังเคราะห์ซิงค์ออกไซด์ด้วยวิธีโซโนเคมี. *Thai Journal of Physics*, 2016. **33**: p. 6-9.
  33. Falk, G.S., et al., *Microwave-assisted synthesis of TiO<sub>2</sub> nanoparticles: photocatalytic activity of powders and thin films*. *Journal of Nanoparticle Research*, 2018. **20**(2).
  34. Ukoba, K.O., A.C. Eloka-Eboka, and F.L. Inambao, *Review of nanostructured NiO thin film deposition using the spray pyrolysis technique*. *Renewable and*

- Sustainable Energy Reviews, 2018. **82**: p. 2900-2915.
35. Tahir, M.B., et al., *Photocatalytic nanomaterials for degradation of organic pollutants and heavy metals*, in *Nanotechnology and Photocatalysis for Environmental Applications*. 2020. p. 119-138.
  36. Safavi, M.S., et al., *Electrodeposited Hydroxyapatite-Based Biocoatings: Recent Progress and Future Challenges*. *Coatings*, 2021. **11**(1).
  37. Cherrington, R. and J. Liang, *Materials and Deposition Processes for Multifunctionality*, in *Design and Manufacture of Plastic Components for Multifunctionality*. 2016. p. 19-51.
  38. Khothong, N., T. Anantamongkolchai, and P. Vas-Umnuay, *Morphology and structure controlled fabrication of Cu<sub>2</sub>ZnSnS<sub>4</sub> thin films by convective assembly deposition*. *Ceramics International*, 2019. **45**(5): p. 6102-6110.
  39. Zhou, Z., et al., *Selective photoelectrocatalytic tuning of benzyl alcohol to benzaldehyde for enhanced hydrogen production*. *Applied Catalysis B: Environmental*, 2021. **286**.
  40. Savari Susila, G. and S. Joseph Selvaraj, *The efficient method for the electrochemical oxidation of benzyl alcohol to benzaldehyde using potassium iodate in a biphasic medium*. *Materials Today: Proceedings*, 2022. **68**: p. 470-477.
  41. Horiguchi, G., et al., *Oxidation of benzyl alcohol using linear paired electrolysis*. *Journal of Environmental Chemical Engineering*, 2022. **10**(3).
  42. Bao, X., et al., *TiO<sub>2</sub>/Ti<sub>3</sub>C<sub>2</sub> as an efficient photocatalyst for selective oxidation of benzyl alcohol to benzaldehyde*. *Applied Catalysis B: Environmental*, 2021. **286**.
  43. Farrag, M. and R. Yahya, *Selective solar photocatalytic oxidation of benzyl alcohol to benzaldehyde over monodispersed Cu nanoclusters/TiO<sub>2</sub>/activated carbon nanocomposite*. *Journal of Photochemistry and Photobiology A: Chemistry*, 2020. **396**.
  44. Higashimoto, S., et al., *Efficient and selective oxidation of benzylic alcohol by O<sub>2</sub> into corresponding aldehydes on a TiO<sub>2</sub> photocatalyst under visible light irradiation: Effect of phenyl-ring substitution on the photocatalytic activity*.

- Journal of Catalysis, 2010. **274**(1): p. 76-83.
45. Lu, M., et al., *Selective oxidation of benzyl alcohol to benzaldehyde with air using ZIF-67 derived catalysts*. Colloids and Surfaces A: Physicochemical and Engineering Aspects, 2021. **629**.
  46. Han, Q., et al., *Mechanism and kinetics of the aerobic oxidation of benzyl alcohol to benzaldehyde catalyzed by cobalt porphyrin in a membrane microchannel reactor*. Chemical Engineering Science, 2021. **245**.
  47. Farivar, F., *CFD simulation and development of an improved photoelectrochemical reactor for H<sub>2</sub> production*. International Journal of Hydrogen Energy, 2016. **41**(2): p. 882-888.
  48. Njoka, F.N., M.A. Ahmed, and S. Ookawara, *Design of a Novel Photoelectrochemical Reactor for Hydrogen Production*, in *Energy and Sustainability VII*. 2017. p. 349-361.
  49. Carver, C., et al., *Modelling and development of photoelectrochemical reactor for H<sub>2</sub> production*. International Journal of Hydrogen Energy, 2012. **37**(3): p. 2911-2923.
  50. Borovinskaya, E.S. and V.P. Reshetilovskii, *Microreactors as the new way of intensification of heterogeneous processes*. Russian Journal of Applied Chemistry, 2011. **84**(6): p. 1094-1104.
  51. Zakaria, M.B., et al., *Preparation of Mesoporous Titania Thin Films with Well-Crystallized Frameworks by Using Thermally Stable Triblock Copolymers*. European Journal of Inorganic Chemistry, 2013. **2013**(13): p. 2330-2335.
  52. Pavan M. V. Raja, A.R.B. *BET Surface Area Analysis of Nanoparticles*. Available from:  
[https://chem.libretexts.org/Bookshelves/Analytical\\_Chemistry/Physical\\_Methods\\_in\\_Chemistry\\_and\\_Nano\\_Science\\_\(Barron\)/02%3A\\_Physical\\_and\\_Thermal\\_Analysis/2.03%3A\\_BET\\_Surface\\_Area\\_Analysis\\_of\\_Nanoparticles#:~:text=%2C%2062%2C%201723.-.Type%20IV%20Isotherm,by%20a%20formation%20of%20multilayers.](https://chem.libretexts.org/Bookshelves/Analytical_Chemistry/Physical_Methods_in_Chemistry_and_Nano_Science_(Barron)/02%3A_Physical_and_Thermal_Analysis/2.03%3A_BET_Surface_Area_Analysis_of_Nanoparticles#:~:text=%2C%2062%2C%201723.-.Type%20IV%20Isotherm,by%20a%20formation%20of%20multilayers.)
  53. Hernández-Granados, A., et al., *Optically uniform thin films of mesoporous TiO<sub>2</sub>*

*for perovskite solar cell applications*. *Optical Materials*, 2019. **88**: p. 695-703.



## VITA

NAME Sirachat Sattayarak

DATE OF BIRTH 30 April 1998

PLACE OF BIRTH Bangkok, Thailand

INSTITUTIONS ATTENDED Chulalongkorn university

HOME ADDRESS 134/3 Tha Sai Subdistrict, Mueang Nonthaburi District, Nonthaburi,  
11000



จุฬาลงกรณ์มหาวิทยาลัย  
CHULALONGKORN UNIVERSITY